Article
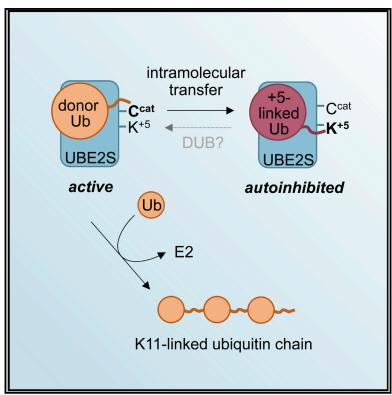
Autoinhibition Mechanism of the Ubiquitin-Conjugating Enzyme UBE2S by Autoubiquitination

Graphical Abstract

Authors

Anna K.L. Liess, Alena Kucerova,
Kristian Schweimer, ...,
Jyoti S. Choudhary, Jörg Mansfeld,
Sonja Lorenz

Correspondence

joerg.mansfeld@tu-dresden.de (J.M.),
sonja.lorenz@
virchow.uni-wuerzburg.de (S.L.)

In Brief

Ubiquitin-conjugating enzymes (E2s) act at the heart of a catalytic cascade that modifies proteins with ubiquitin and regulates countless physiological processes. Liess et al. elucidate the structural basis of a regulation mechanism that seems to be conserved in 25% of human E2s, using UBE2S as a model system.

Highlights

- ~25% of human E2s have a ubiquitination site (Lys^{+5}) near the catalytic center

- Flexibility of the active-site region enables Lys^{+5} autoubiquitination in UBE2S

- Lys^{+5}-linked ubiquitin inhibits UBE2S by adopting a closed conformation

- The extent of Lys^{+5} ubiquitination in UBE2S is regulated during the cell cycle

CellPress

Article

Autoinhibition Mechanism of the Ubiquitin-Conjugating Enzyme UBE2S by Autoubiquitination

Anna K.L. Liess,[1,9] Alena Kucerova,[2,9] Kristian Schweimer,[3] Lu Yu,[4] Theodoros I. Roumeliotis,[4] Mathias Diebold,[5] Olexandr Dybkov,[6] Christoph Sotriffer,[5] Henning Urlaub,[7,8] Jyoti S. Choudhary,[4] Jörg Mansfeld,[2,*] and Sonja Lorenz[1,10,*]

[1]Rudolf Virchow Center for Experimental Biomedicine, University of Würzburg, 97080 Würzburg, Germany
[2]Cell Cycle, Biotechnology Center, Technische Universität Dresden, 01307 Dresden, Germany
[3]Biopolymers, University of Bayreuth, 95447 Bayreuth, Germany
[4]Functional Proteomics Group, The Institute of Cancer Research, London SW3 6JB, UK
[5]Institute of Pharmacy and Food Chemistry, University of Würzburg, 97074 Würzburg, Germany
[6]Department for Cellular Biochemistry, Max Planck Institute for Biophysical Chemistry, Göttingen, 37077 Göttingen, Germany
[7]Group for Bioanalytical Mass Spectrometry, Max Planck Institute for Biophysical Chemistry, Göttingen, 37077 Göttingen, Germany
[8]Proteomics Service Facility, Georg-August-Universität, Göttingen, 37077 Göttingen, Germany
[9]These authors contributed equally
[10]Lead Contact
*Correspondence: joerg.mansfeld@tu-dresden.de (J.M.), sonja.lorenz@virchow.uni-wuerzburg.de (S.L.)
https://doi.org/10.1016/j.str.2019.05.008

SUMMARY

Ubiquitin-conjugating enzymes (E2s) govern key aspects of ubiquitin signaling. Emerging evidence suggests that the activities of E2s are modulated by posttranslational modifications; the structural underpinnings, however, are largely unclear. Here, we unravel the structural basis and mechanistic consequences of a conserved autoubiquitination event near the catalytic center of E2s, using the human anaphase-promoting complex/cyclosome-associated UBE2S as a model system. Crystal structures we determined of the catalytic ubiquitin carrier protein domain combined with MD simulations reveal that the active-site region is malleable, which permits an adjacent ubiquitin acceptor site, Lys^{+5}, to be ubiquitinated intramolecularly. We demonstrate by NMR that the Lys^{+5}-linked ubiquitin inhibits UBE2S by obstructing its reloading with ubiquitin. By immunoprecipitation, quantitative mass spectrometry, and siRNA-and-rescue experiments we show that Lys^{+5} ubiquitination of UBE2S decreases during mitotic exit but does not influence proteasomal turnover of this E2. These findings suggest that UBE2S activity underlies inherent regulation during the cell cycle.

INTRODUCTION

The posttranslational modification of proteins with ubiquitin is a central regulation mechanism in all eukaryotic cells. This requires that ubiquitination itself is tightly regulated. Ubiquitination reactions are driven by a cascade of ubiquitin-activating enzymes (E1), ubiquitin-conjugating enzymes (E2), and ubiquitin ligases

(E3), and are counteracted by deubiquitinases (DUBs). E3s typically mediate substrate recognition and can determine, together with their cooperating E2, which type of modification is formed. Sophisticated mechanisms control the activities of E3s, including interactions with macromolecular or small-molecule ligands, posttranslational modifications, and oligomerization, many of which have been delineated structurally (Buetow and Huang, 2016; Lorenz, 2017; Metzger et al., 2014; Walden and Rittinger, 2018). For example, NEDD8-ylation and associated allosteric changes provide a hallmark activation mechanism in the cullin-RING subfamily (Duda et al., 2011). Moreover, cryo-electron microscopy studies have begun to illuminate how conformational control is implemented in even larger multisubunit E3s, such as the ~1.2-MDa anaphase-promoting complex/cyclosome (APC/C) (Alfieri et al., 2017; Watson et al., 2019). In comparison, how ubiquitination reactions are controlled at the level of E2s is poorly understood.

E2s receive ubiquitin through thioester transfer from an E1 and subsequently cooperate with E3s to catalyze the formation of an isopeptide bond between the C terminus of ubiquitin and a primary amino group of an acceptor protein. In the case of HECT and RBR-type E3s this occurs through an intermediate, which has ubiquitin thioester linked to a catalytic cysteine of the ligase. When cooperating with RING-type E3s, E2s transfer ubiquitin to the acceptor in a single step and can thus directly influence which primary amino group is modified. During RING E3-mediated isopeptide bond formation, the thioester-linked donor ubiquitin adopts a conserved orientation with respect to the catalytic ubiquitin carrier protein (UBC) domain of the E2 that was shown to be stabilized by the RING domain in various E2/E3 systems (Dou et al., 2012; Hamilton et al., 2001; Plechanovová et al., 2012; Pruneda et al., 2012; Saha et al., 2011; Soss et al., 2013; Wickliffe et al., 2011) (Figure S1A). This catalytically critical orientation of the donor ubiquitin toward the E2 is known as a closed state (Pruneda et al., 2011). The positioning of the acceptor protein—a substrate or, alternatively, another ubiquitin molecule—toward the E2-bound donor ubiquitin is often

Table 1. Lys^{+5} Is a Dominant Ubiquitination Site in Human E2s

E2 Enzyme	Total No. of References for All Sites	No. of References for Lys^{+5}	Is Lys^{+5} the Most Detected Site?
UBE2C	83	69	yes
UBE2E1	64	48	yes
UBE2E2	49	49	yes
UBE2E3	48	48	yes
UBE2K	29	8	yes
UBE2N	537	163	yes
UBE2S	35	25	yes
UBE2T	108	90	yes

Proteomic data from the PhosphoSite server (Hornbeck et al., 2015) were analyzed for Lys^{+5} ubiquitination.

supported by additional factors and provides the basis of specificity in substrate modification and ubiquitin linkage formation (Branigan et al., 2015; Brown et al., 2014; Eddins et al., 2006; Kelly et al., 2014; Petroski and Deshaies, 2005; Stieglitz et al., 2013; Wickliffe et al., 2011).

Emerging evidence suggests that E2s use regulatory mechanisms in their own right (Stewart et al., 2016). For example, several members of the E2 family engage ubiquitin noncovalently through their β sheet-containing backside (Bocik et al., 2011; Brzovic et al., 2006; Hibbert et al., 2011; Miura et al., 1999; Page et al., 2012; Ranaweera and Yang, 2013), thereby allosterically activating RING-mediated ubiquitin transfer (Buetow et al., 2015); UBC9, a conjugating enzyme for the ubiquitin-like modifier SUMO, and the ubiquitin-specific E2 UBE2K can be SUMOylated at a common site in the UBC domain, which modulates interactions with substrates and the E1, respectively (Knipscheer et al., 2008; Pichler et al., 2005); UBE2R1, UBE2A, and yeast *UBC2* are phosphorylated in distinct loop regions around the active site with consequences for the conformational dynamics and catalytic activity of the E2 (Coccetti et al., 2008; Papaleo et al., 2011; Sarcevic et al., 2002; Valimberti et al., 2015; Wood et al., 2005); macromolecular interactions and localization of UBE2E3 were found to depend on redox-modifications in the UBC domain (Plafker et al., 2010); and autoubiquitination in the UBC domain or the nonconserved N- and C-terminal extensions have been linked to proteasomal degradation of several E2s (Rape and Kirschner, 2004; Ravid and Hochstrasser, 2007; Sarkari et al., 2013; Williamson et al., 2011) or the suppression of their activities (Banka et al., 2015; Machida et al., 2006). The structural mechanisms by which autoubiquitination modulates the catalytic functions of E2s, however, are unclear.

Here, we address this open question focusing on UBE2S, a cognate E2 of the human APC/C with important roles in mitosis and meiosis (Ben-Eliezer et al., 2015; Garnett et al., 2009; Min et al., 2015; Sako et al., 2014; Wang and Kirschner, 2013; Williamson et al., 2009; Wu et al., 2010), which is overexpressed in a variety of tumors (Ayesha et al., 2015; Chen et al., 2009; Hu et al., 2017; Jung et al., 2006; Li et al., 2018; Liang et al., 2012; Pan et al., 2018; Roos et al., 2011; Tedesco et al., 2007). UBE2S elongates ubiquitin chains on APC/C substrates in a Lys11-linkage-specific manner, following chain initiation by a second APC/C-associated E2, UBE2C (Garnett et al., 2009; Wil-

liamson et al., 2009; Wu et al., 2010). We and others have delineated the interactions of UBE2S with the donor and acceptor ubiquitin, revealing mechanistic peculiarities that render this E2 exquisitely suitable for its APC/C-dependent functions (Brown et al., 2014, 2016; Kelly et al., 2014; Lorenz et al., 2016; Wickliffe et al., 2011): UBE2S has an inherent ability to orient the donor ubiquitin in a closed conformation (Lorenz et al., 2016; Wickliffe et al., 2011) and does not require the RING domain (APC11) for this purpose (Figure S1B). Instead, APC11 functions noncanonically in delivering the acceptor ubiquitin (the distal ubiquitin molecule in a growing, substrate-bound chain) to the catalytic center of UBE2S, thereby promoting processive chain elongation (Brown et al., 2014; Kelly et al., 2014). Moreover, remarkably, the stringent Lys11 specificity of UBE2S in ubiquitin linkage formation is achieved independently of the APC/C through substrate-assisted catalysis (Wickliffe et al., 2011). While the catalytic domain is sufficient for Lys11 linkage specificity (Wickliffe et al., 2011), the lysine-rich C-terminal extension of UBE2S provides autoubiquitination sites and was suggested to mediate the proteasomal turnover of this E2 (Bremm et al., 2010; Williamson et al., 2009; Wu et al., 2010).
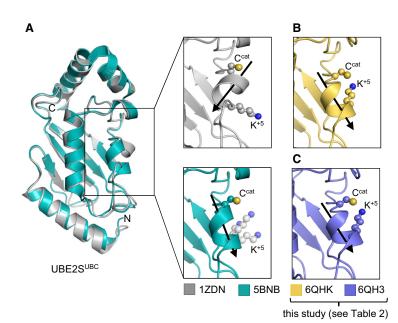
In this study we unravel how the autoubiquitination of a particular lysine (Lys^{+5}) that is situated five residues from the active site in the UBC domain of UBE2S and conserved in ∼25% of human E2s controls catalytic activity. We show that intramolecular transfer of ubiquitin from the catalytic cysteine to Lys^{+5} prevents the E1-mediated reloading of UBE2S with ubiquitin, thus conferring autoinhibition. We observe, intriguingly, that Lys^{+5} ubiquitination of UBE2S is regulated in the context of the cell, with reduced levels during mitotic exit; however, this modification does not trigger proteasomal turnover of UBE2S. Our findings, therefore, suggest that Lys^{+5} ubiquitination provides a regulation mechanism by which the activity of the APC/C may be fine-tuned at the E2 level.
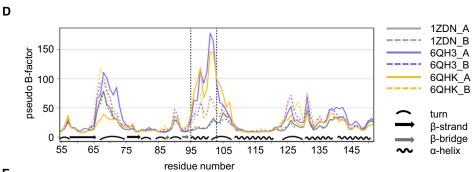
RESULTS

Flexibility of the Active-Site Region of UBE2S Allows for Autoubiquitination of a Conserved Site, Lys^{+5}, in *cis*
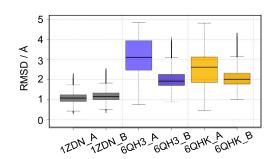
About 25% of the human E2s—UBE2C, UBE2E1, UBE2E2, UBE2E3, UBE2K, UBE2N, UBE2S, and UBE2T—have a conserved lysine residue, Lys^{+5}, situated five residues from the catalytic cysteine (Figure S2). The remaining E2s contain variable amino acids at the +5 position, including Arg, Gln, Glu, Asn, Asp, Ser, Thr, His, and Gly; this implies that neither a lysine nor a positively charged residue at this position presents a conserved catalytic requirement. Remarkably, proteomic data compiled in the PhosphoSitePlus server for posttranslational modifications (Hornbeck et al., 2015) reveal Lys^{+5} as the most detected ubiquitination site in all Lys^{+5}-containing E2s (Table 1), pointing to a common regulatory function of this modification.

To illuminate the structural basis and functional significance of Lys^{+5} ubiquitination we focused on UBE2S. When examining available crystal structures of the catalytic domain (UBE2S^{UBC}), we noticed considerable conformational variability in the region surrounding Lys^{+5}. In one structure (PDB: 1ZDN) (Sheng et al., 2012), Lys^{+5} (Lys100), and the catalytic cysteine (Cys95 or C^{cat}) are located on opposite faces of a short α helix (residues 96–100) that abuts the catalytic center (Figure 1A), their side chains
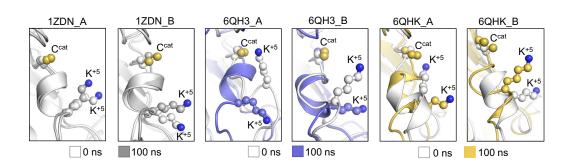
Figure 1. The Active-Site Region of UBE2S Is Conformationally Malleable

(A) Superposition of two crystal structures of UBE2S^{UBC}: PDB: 1ZDN (molecule A, gray) and 5BNB (molecule A, cyan) (left). Details of the active-site region. The side chains of Cys95 (C^{cat}) and Lys100 (K^{+5}) shown in ball-and-stick representation (right). Helical axes are indicated by arrows. In 5BNB, the

(legend continued on next page)

thus being detached from each other. We refer to this state as a Lys^{+5}-*out* conformation. In contrast, a crystal structure of a UBE2S^{UBC}-ubiquitin conjugate (disulfide-linked between C^{cat} and an engineered cysteine at the C terminus of ubiquitin) (PDB: 5BNB) (Lorenz et al., 2016) contains molecules in both Lys^{+5}-*out* (molecules B and C) and Lys^{+5}-*in* (molecules A and D) conformations. In the Lys^{+5}-*in* state the active-site helix is displaced by one residue (comprising residues 97–102) and tilted by 42° compared with the Lys^{+5}-*out* state, thereby enabling the ε-amino group of Lys^{+5} to approach the catalytic center (Figure 1A).

That UBE2S^{UBC} can also adopt a Lys^{+5}-*in* conformation in the absence of ubiquitin is revealed by two new crystal structures that we determined for *apo* UBE2S^{UBC} (Table 2; Figures 1B and 1C). With backbone root-mean-square deviation (RMSD) values of 1.17 and 1.07 Å compared with the previous *apo* structure (PDB: 1ZDN), the catalytic domain adopts a virtually identical fold in these structures (Figures S3A and S3B). The active-site region, however, is arranged into a Lys^{+5}-*in* conformation, as reflected in backbone RMSD values of 2.66 and 2.76 Å, respectively, compared with the previous *apo* structure (Figures S3A–S3D). The observed local conformational changes do not originate from crystal packing, nor does the active-site region engage in lattice contacts in any of the UBE2S^{UBC} *apo* crystals. In this context, it should be mentioned that all three structures (PDB: 1ZDN, 6QHK, and 6QH3) contain a similar crystallographic dimer of UBE2S^{UBC}, although UBE2S was shown to be active as a monomer in solution (Wickliffe et al., 2011). In the original structure (PDB: 1ZDN), the subunits of the crystallographic dimer are linked by a Cys118-mediated disulfide bond (Figure S3E, top); of the newly determined structures, one (PDB: 6QHK) has this disulfide bond replaced by a small-molecule crosslinker (Figure S3E, middle), whereas the other (PDB: 6QH3) contains a UBE2S variant, C118M, that cannot form a covalent linkage at the dimer interface (Figure S3E, bottom). Nevertheless, the dimeric arrangement seen in the three structures is relatively similar (overall backbone RMSD = of 2.96 and 3.18 Å with respect to PDB: 1ZDN; Figure S3E), and, importantly, the common subunit interface is distant from the active-site region. Therefore, our structural analyses suggest that the active-site region of UBE2S can inherently adopt alternative Lys^{+5}-*in* and Lys^{+5}-*out* conformations, indicating local conformational flexibility.

To illuminate this flexibility we performed molecular dynamics simulations using the NAMD 2.12 package (Phillips et al., 2005) with AMBER ff14sb (Maier et al., 2015) forcefield parameters. We carried out two independent 100-ns simulations of each of the three available crystal structures of *apo* UBE2S^{UBC} (PDB: 1ZDN, 6QHK, and 6QH3). The two molecules found in the

asymmetric unit of each of these structures were simulated individually, thus amounting to 12 independent simulations. Collectively, these data show pronounced motions in the active-site region during 200 ns of total simulation time for each molecule, as illustrated by increased backbone root-mean-square fluctuation values (expressed as pseudo B factors) compared with the adjacent α helices (Figure 1D). The distribution of backbone RMSD values of the active-site region (here defined as residues 95–103) supports this idea (Figure 1E) and reveals marked rearrangements of the Lys^{+5}-*in* conformation (seen in PDB: 6QHK and 6QH3), toward the Lys^{+5}-*out* conformation; in contrast, the Lys^{+5}-*out* state (as seen in PDB: 1ZDN) remained rather stable (Figures 1E and 1F). These analyses suggest that the Lys^{+5}-*out* state is energetically favored over the Lys^{+5}-*in* conformation in UBE2S.

To experimentally test for motions of the active-site region in solution we performed steady-state {^{1}H}^{15}N NOE measurements at 18.8 T magnetic field strength. While these experiments did not provide evidence for motions on a picosecond-to-nanosecond timescale (faster than the rotational correlation time of ~10 ns), we observed decreased intensity for several signals in the active-site region in ^{1}H-^{15}N HSQC spectra (data not shown); this supports the notion that the corresponding residues undergo conformational exchange on a timescale that is slower than the one sampled by our {^{1}H}^{15}N NOE experiments.

By definition, the Lys^{+5}-*in* conformation brings the ε-amino group of Lys^{+5} into close proximity to the catalytic center, suggesting that this state is poised for autoubiquitination in *cis*. In contrast, the Lys^{+5}-*out* state is expected to preclude a nucleophilic attack of Lys^{+5} on the C terminus of a ubiquitin molecule linked to the catalytic cysteine of the E2. To test whether ubiquitination of Lys^{+5} occurs preferentially in *cis* or *trans*, we monitored UBE2S autoubiquitination on mixing of an untagged wild-type (WT) and an hemagglutinin (HA)-tagged, catalytically dead, variant (C95A) by anti-HA Western blotting (Figures 2A and 2B). These experiments demonstrate that the autoubiquitination of UBE2S and UBE2S^{UBC} both require ubiquitin transfer in *cis*, even if the active WT protein is provided in excess, in line with previous studies (Bremm et al., 2010).

To ascertain that the autoubiquitination observed *in vitro* involves Lys^{+5} we performed mass spectrometry. We found that Lys^{+5} is, indeed, the predominant autoubiquitination site in UBE2S^{UBC} and also modified in UBE2S (Table 3). In the full-length protein, additional modifications map to the lysine-rich C-terminal extension, of which only few sites (e.g., Lys197 and Lys198) can be identified by tryptic digest-based methods,

three most likely rotamers of the K^{+5} side chain are shown (white), since it was not modeled in the structure. The C^{cat}-linked ubiquitin in 5BNB is not displayed for clarity.

(B and C) Analogous detail of the active-site region in the crystal structures of UBE2S^{UBC} WT (PDB: 6QHK; yellow) (B) and UBE2S^{UBC} C118M (PDB: 6QH3; blue) (C), determined in this study.

(D) Results of molecular dynamics simulations (200 ns total sampling) with the two unique molecules (A and B) found in each of the three crystal structures of *apo* UBE2S^{UBC} (PDB: 1ZDN, 6QH3, and 6QHK). Per-residue backbone root-mean-square fluctuation values in relation to the averaged structure are displayed as pseudo B-factors. For details, see the STAR Methods. The active-site region (residues 95–103) is marked by dotted lines. Secondary structure elements for (PDB: 1ZDN), determined by STRIDE (Heinig and Frishman, 2004), are indicated.

(E) Distribution of backbone RMSD values during 200 ns of simulation for the active-site region (defined as in (D)) of each of the 6 molecules compared with the corresponding starting structures.

(F) Snapshots of the active-site region during the simulations. Each panel shows a superposition of the equilibrated structure (0 ns; white) and the state after 100 ns of simulation (colored), with the side chains of C^{cat} and K^{+5} shown in ball-and-stick representation.

Table 2. X-Ray Crystallographic Data Collection and Refinement

	UBE2S^{UBC} WT (PDB: 6QHK)	UBE2S^{UBC} C118M (PDB: 6QH3)
Data Collection		
Wavelength	0.9680	0.9762
Space group	P 6$_5$	P 6$_5$
Unit cell parameters		
a, b, c (Å)	83.15, 83.15, 83.13	84.62, 84.62, 87.83
α, β, γ (°)	90, 90, 120	90, 90, 120
Total reflections	46,726 (4,620)	15,965 (1,589)
Unique reflections	23,393 (2,317)	7,984 (795)
R$_{pim}$	2.32 (28.1)	2.63 (17.29)
Completeness (%)	99.72 (99.44)	99.94 (100.00)
I/σ(I)	20.05 (2.64)	21.40 (4.19)
Redundancy	2.0 (2.0)	2.0 (2.0)
Wilson B factor	32.04	63.58
CC½	1 (0.938)	0.999 (0.896)
Refinement		
Resolution (Å)	19.42–1.96 (2.03–1.96)	38.12–2.90 (3.004–2.90)
R$_{work}$/R$_{free}$	18.93/22.34	18.47/22.89
No. of atoms	2,364	2,270
Protein	2,253	2,270
Water	84	
Average B factors	39.11	67.17
Protein	39.16	67.17
Water	35.65	
RMSD from ideality		
Bond lengths (Å)	0.003	0.004
Bond angles (°)	0.7	0.80
Ramachandran statistics (%)		
Favored	98.63	98.28
Disallowed	0.00	0.00
MolProbity clash score	1.77	13.24
MolProbity overall score	0.93	1.63

X-ray crystallographic data collection and refinement statistics for the structures of UBE2S^{UBC} WT (PDB: 6QHK) and C118M (PDB: 6QH3). Values in parentheses correspond to the highest-resolution shell. RMSD, root-mean-square deviation.

owing to the accumulation of positively charged residues in this region.

Consistent with a dominant modification of the C-terminal extension, the mutation of Lys^{+5} to arginine does not visibly affect the overall autoubiquitination pattern of UBE2S in vitro (Figure S4A). In contrast, the same mutation markedly reduces autoubiquitination in the context of UBE2S^{UBC} (Figure S4B). A comparison of reactions supplemented with ubiquitin WT and K11R demonstrates that UBE2S and UBE2S^{UBC} are modified with Lys11-linked chains (Figures S4A and S4B); at least in the context of UBE2S^{UBC}, those include chains assembled on Lys^{+5} (Figure S4B). However, we will show in the following section that Lys^{+5} ubiquitination inhibits UBE2S. Our observations,

therefore, imply that chain elongation on Lys^{+5} occurs in trans; yet, autoubiquitination of UBE2S generally ought to be initiated in cis (Figure 2).

Lys^{+5} Ubiquitination of UBE2S Confers Autoinhibition

To dissect the functional consequences of Lys^{+5} ubiquitination we set out to isolate UBE2S exclusively modified at this site. Since full-length UBE2S extensively autoubiquitinates its C-terminal extension (Figure S4A), we purified the monoubiquitinated form of UBE2S^{UBC} (UBE2S^{UBC}-Ub) from an in vitro reaction supplied with ubiquitin K11R. That this conjugate had ubiquitin predominantly attached to Lys^{+5} was confirmed by mass spectrometry ($\sim$95% Lys^{+5}-linked conjugate detected; Table S1). We next subjected the purified conjugate to activity assays, monitoring the individual reaction steps of ubiquitin thioester formation and isopeptide bond formation. These experiments reveal that Lys^{+5} ubiquitination of UBE2S^{UBC} strongly impairs thioester formation with ubiquitin ($\sim$85% reduction compared with the unmodified enzyme) (Figure 3A). It remains unclear whether the residual amount of thioester- and isopeptide-linked reaction product ((UBE2S^{UBC}-Ub)$\sim$Ub) carried ubiquitin at Lys^{+5} or whether it originated from the small input amount of UBE2S^{UBC}-Ub linked through an alternative lysine residue ($\sim$5% K68-linked conjugate detected; Table S1).

In line with the observed defect in ubiquitin thioester formation, Lys^{+5}-modified UBE2S^{UBC} also lost isopeptide bond formation activity, as monitored by virtue of the diubiquitin reaction product (Ub$_2$) and visualized by Coomassie staining (Figure 3B, left, top image); using more sensitive near-infrared fluorescence imaging as a readout, a small amount of Ub$_2$ is detectable (Figure 3B, left, bottom image; quantified on the right), consistent with the residual amount of ubiquitin thioester formation. Taken together, transferring ubiquitin to Lys^{+5} strongly autoinhibits UBE2S at the stage of ubiquitin thioester formation.

Lys^{+5}-Linked Ubiquitin Adopts a Closed Orientation toward UBE2S

To unravel the mechanistic basis of the Lys^{+5} ubiquitination-induced inhibition of UBE2S we characterized the orientation of Lys^{+5}-linked ubiquitin toward the catalytic domain. Previous work showed that the thioester-linked donor ubiquitin adopts a catalytically critical, closed orientation toward a number of E2s, including UBE2S (Dou et al., 2012; Hamilton et al., 2001; Plechanovová et al., 2012; Pruneda et al., 2011, 2012; Saha et al., 2011; Soss et al., 2013; Wickliffe et al., 2011). Whereas this conformation is stabilized by the RING domain in canonical E2/RING E3 systems (Dou et al., 2012; Plechanovová et al., 2012; Pruneda et al., 2012) (Figure S1A), UBE2S can position the donor ubiquitin in a closed state in the absence of the APC/C and even in trans (Lorenz et al., 2016; Wickliffe et al., 2011) (Figure S1B). Interestingly, structural modeling suggested that ubiquitin adopts a conformation similar (but likely not identical) to the closed state during thioester transfer from the E1 to the E2 (Olsen and Lima, 2013).

Based on the proximity of the catalytic cysteine to Lys^{+5} in the E2 and the flexibility of the C-terminal tail of ubiquitin, we hypothesized that ubiquitin may still adopt a closed orientation on conjugation to Lys^{+5}. If so, Lys^{+5}-linked ubiquitin would obstruct a productive, closed arrangement of donor ubiquitin during
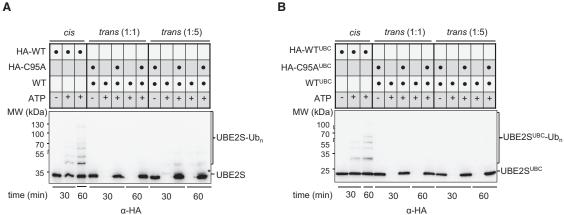
Figure 2. UBE2S Autoubiquitination Occurs in *cis*

(A) *Cis/trans* assay monitoring the ubiquitination of 1 μM HA-tagged UBE2S (HA-WT) and 1 μM HA-tagged, catalytically dead UBE2S (HA-C95A) in the presence of untagged WT UBE2S (at molar ratios of 1:1 and 1:5), respectively. Reactions were monitored over 30 and 60 min and visualized by SDS-PAGE and anti-HA Western blotting. Ubiquitinated UBE2S species are denoted as UBE2S-Ub$_n$. The asterisk marks a background signal.

(B) Analogous assay as in (A) using the catalytic domain of UBE2S, UBE2S^{UBC}.

E1-mediated thioester transfer, as we observed experimentally. To test this idea we investigated Lys^{+5}-ubiquitinated UBE2S^{UBC} by NMR. Due to the considerable amount of isotope-enriched material required for these studies, protein conjugates were not prepared enzymatically in this case. Instead, we introduced a disulfide linkage between Cys76 of ubiquitin (G76C variant) and Cys^{+5} of a UBE2S^{UBC} variant (C95S/K100C/C118M), whereby the two native cysteine residues (C^{cat} and Cys118) had been mutated (Figure 4A). We replaced Cys118 by methionine, because this substitution had previously been shown to leave the closed UBE2S-donor ubiquitin interaction intact (Lorenz et al., 2016). The required backbone resonance assignments for the mutated UBE2S^{UBC} variant and the +5-modified conjugate with ubiquitin were generated with the help of triple resonance experiments (for details, see the STAR Methods).

To understand how Lys^{+5}-linked ubiquitin interacts with UBE2S^{UBC} we recorded ^{1}H-^{15}N HSQC spectra of conjugates with either the E2 or the ubiquitin component ^{15}N enriched (Figure 4A), and analyzed the chemical shift perturbations, $\Delta\delta(^1H^{15}N)$, with respect to the spectra of the corresponding *apo* proteins (Figures 4B and 4C). In ubiquitin, major perturbations ($\Delta\delta(^1H^{15}N) > 0.1$ ppm) map to the C-terminal tail (residues 70–76), with which ubiquitin is anchored at the UBE2S active site, and an adjacent region surrounding the notorious hydrophobic patch. This pattern of perturbations bears striking resemblance to the binding site used by UBE2S-bound donor ubiquitin (Lorenz et al., 2016; Wickliffe et al., 2011). In fact, several of the identified residues in this site, including Leu8, Lys48, His68, Val70, Leu71, and Arg72, provide key contacts in the closed donor conformation (Figure 4D) (Wickliffe et al., 2011).

Consistently, major chemical shift perturbations in +5-modified UBE2S^{UBC} also coincide with the closed donor ubiquitin binding site; functionally validated key residues in this region include Glu51, Cys118, and Ile121, as well as Arg101 and Asp102, near the active site (Figure 4E). Figure S5 shows a comparison of the chemical shift perturbations induced in UBE2S^{UBC} on conjugation of ubiquitin to the +5 position and the active-site

position (oxyester linkage to a C95S variant of UBE2S^{UBC}, as studied previously [Wickliffe et al., 2011]). The two profiles match closely, corroborating the idea that the Lys^{+5}-linked ubiquitin adopts a donor-like, closed orientation toward UBE2S.

It should be noted that a second set of chemical shift perturbations specifically induced by Lys^{+5}-linked ubiquitin is observed at the rim of the β sheet that flanks the catalytic center of UBE2S opposite the closed donor binding site (Figures 4E and S5). These perturbations likely reflect propagated changes in the chemical environment on linkage of ubiquitin to Lys^{+5}; however, we cannot rule out the possibility that they arise from an alternative binding mode of ubiquitin, in addition to the closed conformation. Either way, our NMR analyses demonstrate that Lys^{+5}-linked ubiquitin can interact with UBE2S in a manner that mimics the donor ubiquitin, thereby competing with a

Table 3. Autoubiquitination Sites of UBE2S *In Vitro*

Gly-Gly-Lys Site Detected	MS1 Intensity		PSMs	
	UBE2S^{UBC}	UBE2S	UBE2S^{UBC}	UBE2S
18	1.94E+08	1.49E+08	2	1
68	2.98E+08	2.64E+08	1	1
76	1.30E+08	1.01E+08	2	2
82	6.06E+07	4.31E+07	2	1
100 (= Lys^{+5})	**8.55 × 10^9**	**7.02 × 10^9**	**47**	**15**
117	9.34E+07	4.45E+07	3	1
197	**0**	**9.43 × 10^9**	**0**	**15**
198	**0**	**9.43 × 10^9**	**0**	**19**

Semi-quantitative mass spectrometric analysis of *in vitro* autoubiquitination sites in UBE2S, based on a MaxQuant (Tyanova et al., 2015) search for Lys-Gly-Gly modifications, following tryptic digest, against the human SwissProt database (UniProt Consortium T, 2018). The MS1 (mass spectrum 1) intensity typically correlates well with peptide abundance in the sample; PSMs (peptide spectrum matches) are also shown and, while not providing a reliable quantitative readout, reflect the same trend. Major modification sites (K100 [Lys^{+5}], K197, and K198) are highlighted in bold.
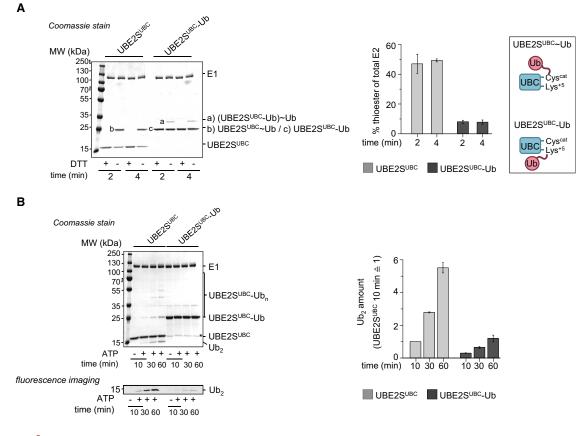
Figure 3. Lys^{+5} Ubiquitination of UBE2S Confers Autoinhibition

(A) Comparison of the abilities of UBE2S^{UBC} and purified Lys^{+5}-ubiquitinated UBE2S^{UBC} (UBE2S^{UBC}-Ub) to accept ubiquitin from the E1 (thioester transfer assay). The thioester linkage, denoted as "∼," is sensitive to reducing agent (DTT). Two time points, as indicated, were monitored by SDS-PAGE and Coomassie staining (left). The amounts of UBE2S^{UBC}∼Ub and (UBE2S^{UBC}-Ub)∼Ub were quantified, normalized to the input amount of unmodified enzyme (plus DTT lane), and the mean and SD from three independent experiments plotted (middle). A cartoon is shown to clarify the nomenclature (right).

(B) Comparison of the abilities of UBE2S^{UBC} and purified Lys^{+5}-ubiquitinated (UBE2S^{UBC}-Ub), see (A), to promote ubiquitin isopeptide bond formation using fluorophore-labeled ubiquitin. Three time points, as indicated, were monitored by SDS-PAGE and Coomassie staining (left, top image) or fluorescence imaging (left, bottom image). The asterisk marks a small amount of contaminating UBE2S^{UBC} in the UBE2S^{UBC}-Ub preparation. The amount of diubiquitin (Ub$_2$), monitored by fluorescence imaging was quantified, and the mean and SD from three independent experiments plotted; the amount of Ub$_2$ formed by UBE2S^{UBC} after 10 min was set to 1 (right). Note that, in both (A and B), we compared UBE2S^{UBC} and UBE2S^{UBC}-Ub recovered from the same reaction. In that way, we ensured that the enzymes had been treated consistently throughout the preparation procedure.
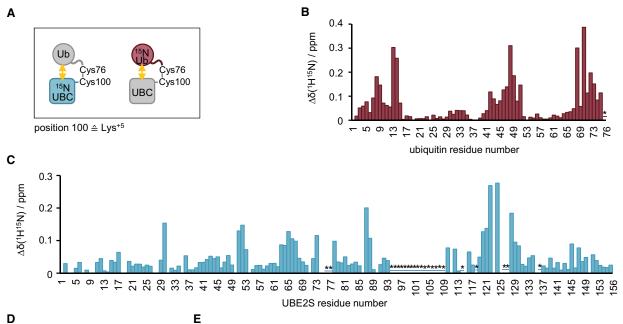
productive positioning of ubiquitin during thioester transfer from the E1 and conferring autoinhibition (Figures 4F and 4G).
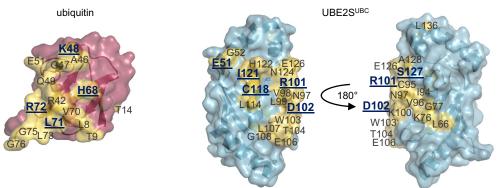
Autoubiquitination of UBE2S Primarily Occurs at the C-Terminal Extension *In Vitro*

Since the autoubiquitination of Lys^{+5} shuts down UBE2S activity, we reckoned that its occurrence must be either suppressed or tightly regulated in order to prevent inadvertent accumulation of inactive UBE2S in the cell. We initially interrogated this idea based on E3-independent *in vitro* activity assays. As noted above, the overall autoubiquitination pattern of full-length UBE2S seems to be largely unaffected by the mutation of Lys^{+5} to arginine (Figure S4A), despite ∼40% of UBE2S being modified within 60 min of reaction time (Figures 5A, 5B, and S6A). Consistently, UBE2S WT and K^{+5}R assemble free ubiquitin chains (monitored by virtue of Ub$_2$) with similar efficiency (Figure 5A). We next investigated whether Lys^{+5} ubiquitination-induced inhibition of UBE2S can be detected in the context of

reconstituted APC/C-dependent reactions, using an N-terminal fragment of cyclin B1 fused to ubiquitin as a model substrate (Ub-cyclin B1) (Brown et al., 2014). This fusion protein bypasses the need to supplement the reactions with an additional chain-initiating E2 (UBE2C), thereby providing a selective readout of UBE2S-mediated chain elongation. Analogous to the E3-independent reactions, these studies show that the UBE2S WT and K^{+5}R variants promote substrate ubiquitination with the same efficiency (Figures 5C and 5D) and appear to be autoubiquitinated to a similar degree (Figures S6B and S6C). Thus, the inhibition of the small fraction of Lys^{+5}-modified UBE2S is not detectable in our *in vitro* setup, whereby ubiquitin chain formation at the C-terminal extension dominates over Lys^{+5} ubiquitination.

In an attempt to artificially boost the fraction of Lys^{+5}-modified UBE2S *in vitro*, we mutated the two autoubiquitination sites that we had identified as ubiquitin acceptors within the C-terminal extension. However, the UBE2S K197R/K198R variant was still modified with ubiquitin chains on residues other than Lys^{+5},
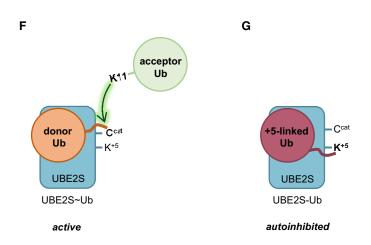
Figure 4. Lys^{+5}-Linked Ubiquitin Adopts a Donor-like, Closed Orientation toward UBE2S

(A) Cartoon of two UBE2S^{UBC}-ubiquitin conjugates, mimicking Lys^{+5}-ubiquitinated UBE2S^{UBC} (UBE2S-Ub). They contain an engineered single-cysteine variant of UBE2S^{UBC} (C95S/C118M/K100C) disulfide-linked to a cysteine-containing ubiquitin variant (G76C). For chemical shift mapping by NMR, either the E2 (blue) or the ubiquitin (red) component was ^{15}N-enriched, while the second component was unlabeled (gray).

(legend continued on next page)

indicating that additional lysine residues in the C-terminal extension act as ubiquitin acceptors, but escape detection by tryptic digest-based mass spectrometry (Figures S7A and S7B). Finally, we used ubiquitin K11R in lieu of the WT in order to prevent chain formation, but did not observe a pronounced effect of Lys^{+5} in this context either (Figures S7C and S7D). Analogous results were obtained in APC/C-dependent reactions (Figure S8). When studying minimalized recombinant conjugation systems *in vitro*, autoubiquitination at Lys^{+5} is thus underrepresented compared with sites in the C-terminal extension of UBE2S. In principle, this is consistent with the notion that the active-site region of UBE2S inherently favors the Lys^{+5}-*out* state (Figures 1E and 1F), thereby preventing autoubiquitination at Lys^{+5}. That residues in the C-terminal extension are readily modified reflects the high concentration of lysine residues in this region and, possibly, the proximity of these residues to the catalytic center.

Lys^{+5} Ubiquitination of UBE2S Is Prominent in the Cell and Regulated

Although Lys^{+5} ubiquitination of UBE2S and, therefore, autoinhibition, is not a dominant event *in vitro*, a large body of proteomic analyses has identified Lys^{+5} as a prevalent modification site in the context of the cell (Table 1), suggesting a regulatory function of this modification. We thus investigated the extent and time point of Lys^{+5} ubiquitination of UBE2S during mitosis. To enrich UBE2S for mass spectrometric analyses we raised a polyclonal antibody against recombinant UBE2S^{UBC} and characterized the specificity of this reagent. Western blotting, combined with mass spectrometry (Table S2), demonstrates that the affinity-purified antibody precipitates endogenous unmodified UBE2S as well as ubiquitinated forms from prometaphase-arrested HeLa K cells, while showing cross-reactivity with the mitotic checkpoint protein MAD1 (Figures 6A and S9A). Moreover, the antibody recognizes mono- and polyubiquitinated UBE2S species with similar efficiency as the anti-ubiquitin antibody P4D1 (Figure S9B). Intriguingly, quantitative Western blot analysis reveals that almost 40% of the immunoprecipitated UBE2S in prometaphase is monoubiquitinated (Figure 6B), identifying monoubiquitination as a dominant modification state in the context of the cell.

Since the activity of the APC/C is precisely regulated during mitosis, we next investigated whether the ubiquitination state of UBE2S varies during mitotic exit. To this end HeLa K cells were synchronized in prometaphase by treatment with the microtubule-stabilizing drug taxol and collected by mitotic shake-off (0-min time point). Subsequently, cells were released from the drug-induced arrest into fresh medium for 30 and 120 min, respectively, to allow for mitotic exit (Figure 6C). Quantitative Western blot analyses show that UBE2S monoubiquitination remains constant over 30 min after release, which recapitulates a meta/anaphase-like stage; in contrast, the fraction of monoubiquitinated UBE2S strongly decreases toward the end of mitotic exit (120-min time point) (Figures 6D and 6E).

To determine whether the observed change in UBE2S mono-ubiquitination is mirrored by differences in the ubiquitination level of Lys^{+5}, we performed quantitative tandem mass tag mass spectrometry (Thompson et al., 2003). Based on the abundance of Lys^{+5}-ubiquitinated peptides relative to all unmodified UBE2S-derived peptides (Figures 6F and 6G; Table S3), we observed, indeed, a 2-fold drop in Lys^{+5} ubiquitination 120 min after release compared with the earlier time points (Figure 6H). Note that a quantitative comparison of the fraction of UBE2S ubiquitinated at Lys^{+5} and alternative sites was not possible, owing to the multiplexed experimental design. Nevertheless, the high abundance of monoubiquitinated UBE2S and the striking correlation of the dynamics of monoubiquitinated and Lys^{+5}-ubiquitinated UBE2S over time indicate that Lys^{+5} ubiquitination may play a significant role in the regulation of UBE2S during mitosis.

Our analyses further reveal that the total level of UBE2S decreases during mitotic exit (Figures 6D and 6F), possibly reflecting autoubiquitination-dependent proteasomal degradation of this E2 (Williamson et al., 2009). To test whether Lys^{+5} ubiquitination contributes to the degradation of UBE2S we generated isogenic tetracycline-inducible hTERT-immortalized retina pigment epithelial cell lines (RPE-1) expressing untagged small interfering RNA (siRNA)-resistant UBE2S WT or $K^{+5}R$ from the same mRNA as EGFP to monitor protein expression. Next, we efficiently depleted endogenous UBE2S by siRNA for 48 h, induced the expression of UBE2S WT or $K^{+5}R$, and determined UBE2S stability in the presence of the translation inhibitor cycloheximide and the proteasome inhibitor MG132. These studies demonstrate that the stability of UBE2S WT and $K^{+5}R$ depends on proteasomal activity; however, both variants are turned over with similar kinetics in the absence of MG132, indicating that Lys^{+5} ubiquitination is not a major determinant of UBE2S stability (Figure 7). Hence, a nondegradative mechanism controls the abundance of Lys^{+5}-ubiquitinated UBE2S in the cell.

(B) Weighted combined chemical shift perturbations, $\Delta\delta(^1H^{15}N)$, of ubiquitin resonances in the context of the covalently linked conjugate with UBE2S^{UBC} compared with the *apo* protein, plotted over the ubiquitin residue number. The asterisk denotes line broadening.

(C and D) (C) Weighted combined chemical shift perturbations, $\Delta\delta(^1H^{15}N)$, of UBE2S resonances in the context of the covalently linked conjugate with ubiquitin compared with the *apo* protein, plotted over the UBE2S residue number. Asterisks indicate line broadening and/or signal disappearance due to chemical exchange on the intermediate chemical shift timescale. Gaps are due to proline residues (9, 10, 27, 28, 35, 50, 54, 71, 74, 75, and 86) or missing assignments (for details, see the STAR Methods). (D) Combined cartoon and surface representation of the crystal structure of ubiquitin (PDB: 1UBQ) (Vijay-Kumar et al., 1987). Residues that undergo marked chemical shift perturbations ($\Delta\delta(^1H^{15}N) > 0.1$ ppm) or line broadening in the context of the conjugate with UBE2S^{UBC}, see (B), are highlighted in yellow. Residues labeled bold are functionally validated key contacts in the closed UBE2S-donor ubiquitin interface, as reported in previous studies (Wickliffe et al., 2011).

(E) Analogous representation as in (D) for UBE2S, using the crystal structure of UBE2S^{UBC} (PDB: 1ZDN; Sheng et al., 2012, shown in two orientations) and a cut-off of $\Delta\delta(^1H^{15}N) > 0.12$ ppm. Note that N87 of UBE2S is buried.

(F) Cartoon model of the active state of UBE2S: the donor ubiquitin is thioester-linked to the active site (C^{cat}), adopts a closed conformation with respect to the E2, and is nucleophilically attacked by Lys11 of the acceptor ubiquitin.

(G) Cartoon model of the identified autoinhibited state of UBE2S: ubiquitin is isopeptide-linked to Lys^{+5} of the E2, thus preventing the reloading of the active site with ubiquitin.
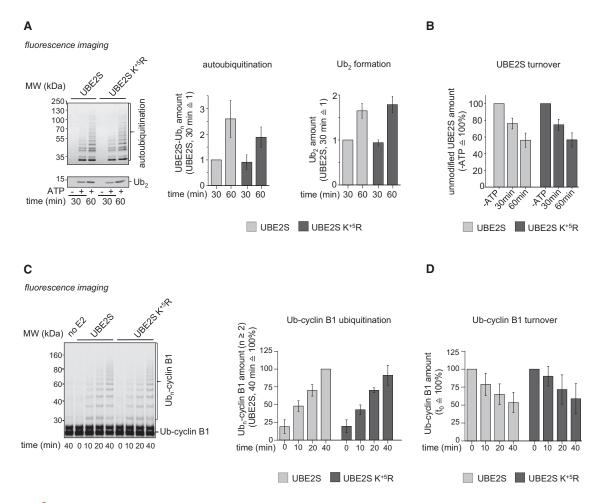
Figure 5. Lys^{+5} Ubiquitination of UBE2S Occurs Primarily at the C-terminal Extension *In Vitro*

(A) Comparison of the isopeptide bond formation activities of UBE2S WT and K^{+5}R in E3-independent *in vitro* reactions, supplemented with fluorophore-labeled ubiquitin. Autoubiquitinated UBE2S (UBE2S-Ub$_n$) and Ub$_2$ were monitored by fluorescence imaging at two time points, as indicated. Note that two images are shown for the respective reaction products, owing to differences in their relative intensities (left). The amounts of reaction products were quantified, and the mean and SD from three independent experiments plotted; the amount of reaction product formed by WT UBE2S after 30 min was set to 1 (middle, right).

(B) Analogous quantification of the residual amounts of unmodified UBE2S variants (WT and K^{+5}R), based on SDS-PAGE and Coomassie staining (Figure S5A), normalized to the input amount of enzyme (minus ATP lane set to 100%).

(C) Comparison of the activities of UBE2S WT and K^{+5}R toward a fluorophore-labeled ubiquitin-cyclin B1 fusion substrate (Ub-cyclin B1) (for details, see the STAR Methods) in the presence of recombinant APC/C, monitored by SDS-PAGE and fluorescence imaging (left). The amount of ubiquitinated substrate was quantified at different time points, as indicated, normalized to the amount of product formed by WT UBE2S after 40 min (100%), and the mean and SD from three independent experiments were plotted (right).

(D) Analogous quantification of the amounts of unmodified substrate, normalized to the input amount of substrate (time point zero set to 100%).

DISCUSSION

This study provides structural, mechanistic, and cell-based evidence of the emerging notion that E2s have evolved inherent mechanisms to keep their activities in check, thus fine-tuning ubiquitin-mediated signaling responses. We show that the intramolecular autoubiquitination of UBE2S at Lys^{+5} provides efficient autoinhibition by interfering with the E1-mediated transfer of ubiquitin to the E2. Our finding that Lys^{+5}-linked ubiquitin can adopt a closed orientation with respect to UBE2S provides a structural rationale for this effect (Figures 4F and 4G): the Lys^{+5}-linked ubiquitin competes with the productive positioning of the donor ubiquitin, which was suggested to adopt a closed-type orientation during thioester transfer (Olsen and Lima, 2013).

The attachment of ubiquitin to Lys^{+5} is also expected to affect the chemical environment and reactivity of the adjacent catalytic center toward the donor-E1 complex, and may hinder ubiquitin transfer sterically. Notably, these mechanisms are independent of the acceptor ubiquitin and may apply to any Lys^{+5}-containing E2, regardless of its linkage specificity or processivity in chain formation. We thus posit that autoubiquitination of Lys^{+5} provides a common inhibitory mechanism in functionally diverse E2s, in line with the observation that Lys^{+5} ubiquitination mediates inhibition of the mono-ubiquitinating UBE2T (Machida et al., 2006), in addition to the chain-elongating UBE2S. Indeed, Lys^{+5} is conserved in ~25% of the human E2 enzymes, but its mutation to arginine does not affect catalysis in several cases (Bakos et al., 2018; Banka et al., 2015; Middleton and Day,
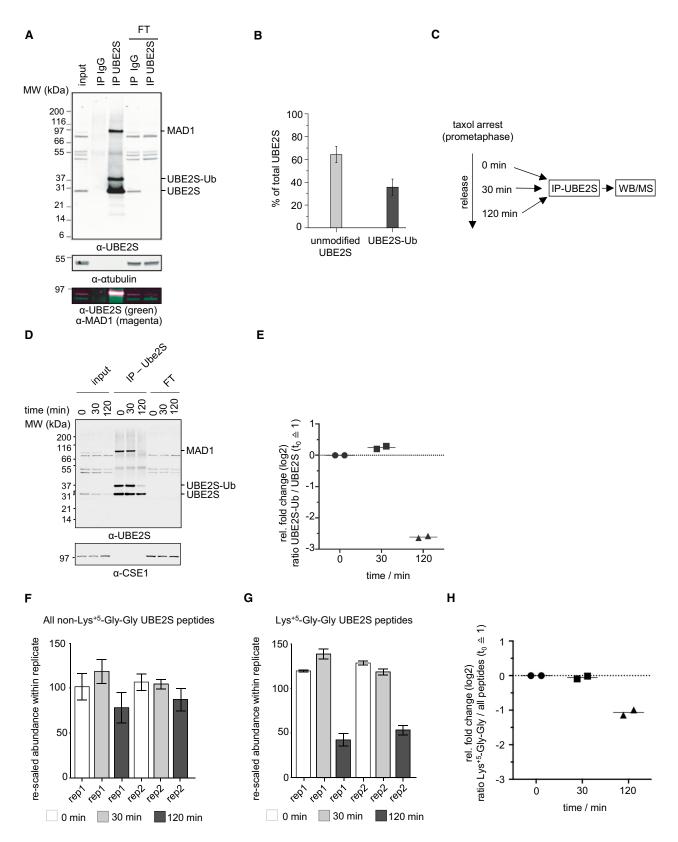
Figure 6. Lys^{+5} Ubiquitination of UBE2S Is Cell Cycle-Dependent

(A) Representative Western blot analysis of input, control (immunoglobulin G), and UBE2S immunoprecipitations from prometaphase-arrested HeLa K cells, and the corresponding flow-throughs (FT). To preserve UBE2S-ubiquitin conjugates, cells were extracted in the presence of iodoacetamide and MG132 to inhibit
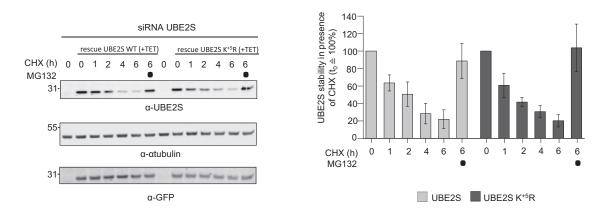
(legend continued on next page)

Figure 7. Lys^{+5} Ubiquitination Does Not Induce Proteasomal Degradation of UBE2S

Representative Western blot analysis of RPE-1 cells expressing UBE2S and UBE2S K^{+5}R on tetracycline induction (±TET), treated with 355 μM cycloheximide (CHX) or with 10 μM MG132 at different time points, as indicated (left). α-Tubulin serves as a loading control, GFP as an expression control. Quantification of the relative levels of UBE2S, based on Western blotting and near-infrared fluorescence imaging. The mean and SD from four independent experiments were plotted (right).

2015). This argues for a conserved regulatory function of Lys^{+5} and against the idea that ubiquitination at this site constitutes a fortuitous dead end.

For Lys^{+5} ubiquitination-mediated regulation to take effect, the inhibited step of ubiquitin-E2 thioester formation needs to be rate-limiting in the corresponding cellular pathway. Interestingly, this may, indeed, be the case for UBE2S, which elongates ubiquitin chains on APC/C substrates with high processivity (Garnett et al., 2009; Wickliffe et al., 2011; Williamson et al., 2009; Wu et al., 2010); yet the positioning of UBE2S on the APC/C is incompatible with a simultaneous engagement of the E1 for reloading of the E2 with ubiquitin. To resolve this problem, it has been speculated that rapid reloading may occur through exclusive release of the catalytic UBC domain of UBE2S from APC2, while its C-terminal extension remains anchored on the APC/C platform (Brown et al., 2014). A conceptually similar mechanism was proposed for yeast *UBC1*, whose UBA domain may provide an APC/C anchor, allowing the catalytic domain to cycle between alternative interactions with the E1 and E3 (Girard et al., 2015). Although different in structural detail, these mechanisms are expected

to enhance the residence time of a single chain-elongating E2 molecule on the E3 and render the system exquisitely sensitive to Lys^{+5} ubiquitination-mediated inhibition of E1-mediated reloading of this E2 molecule.

The close proximity of Lys^{+5} to the catalytic center and the conformational malleability of the active-site region, however, bear the inherent risk of inadvertent Lys^{+5} ubiquitination and resulting inactivation of the E2. Therefore, the occurrence of this modification must be tightly regulated in the cell. Intriguingly, our studies demonstrate that the fraction of Lys^{+5}-ubiquitinated UBE2S is, indeed, dynamic with a marked drop during mitotic exit. At the same time, the total level of UBE2S decreases, indicating a carefully tuned balance of UBE2S abundance and activity. While the physiological origin and consequences of this balance remain to be determined, our observations imply that cell-cycle-dependent factors control the autoubiquitination of UBE2S at Lys^{+5}. In principle, these factors may include macromolecular interaction partners that influence the conformation of the active-site region of UBE2S directly or allosterically, thereby modulating the ability of Lys^{+5} to serve as a ubiquitin acceptor. For example, conformational changes of

DUBs and proteasome activity, respectively. Note, the polyclonal anti-UBE2S antibody also recognizes and precipitates MAD1 (green/magenta overlay). α-Tubulin serves as a loading control.

(B) Quantification of the relative levels of unmodified and monoubiquitinated UBE2S in prometaphase-arrested cells, determined from immunoprecipitations as shown in (A), based on Western blotting and near-infrared fluorescence imaging. The mean and SD from three independent experiments were plotted.

(C) Schematic representation of the cell synchronization scheme used to analyze UBE2S ubiquitination dynamics during mitosis.

(D) Representative Western blot analysis (n = 2) of UBE2S immunoprecipitations from cells released from taxol-induced prometaphase arrest for 0, 30, and 120 min, as illustrated in (C). CSE1 serves as a loading control.

(E) Analysis of the relative change in UBE2S monoubiquitination based on immunoprecipitations, as shown in (D), by Western blotting and near-infrared fluorescence-based quantification. The mean and single data points from two independent experiments (normalized to t_0) were plotted.

(F) Relative abundances of nonmodified UBE2S peptides determined by tandem mass tag (TMT)-mass spectrometry from the same samples as analyzed in (D). The mean and SD from two independent experiments, based on 20 identified unmodified UBE2S peptides (13 unique) were plotted. Note, the relative abundance of unmodified UBE2S decreases by ~20% 120 min after release.

(G) Relative abundances of Lys^{+5}-ubiquitinated UBE2S peptides determined by TMT-mass spectrometry from the same samples as analyzed in (D). The mean and SD from two independent experiments, based on two identified ubiquitinated Lys^{+5} UBE2S peptide forms (with and without deamidation) and normalized to t_0 were plotted. Note, the relative abundance of Lys^{+5}-ubiquitinated UBE2S decreases by ~65% 120 min after release compared with the samples taken at 0 and 30 min.

(H) Quantification of the relative change in Lys^{+5}-Gly-Gly UBE2S peptides, based on the data shown in (F and G). Lines indicate the mean from two independent experiments.

the APC/C, as triggered by the availability or identity of substrates, the length of the assembled, substrate-bound ubiquitin chains, or posttranslational modifications, may be propagated to the UBE2S active site. It is also conceivable that Lys^{+5} ubiquitination is influenced by the C-terminal extension of UBE2S, depending on its conformation and the dynamics of its association with the APC/C. Remarkably, the APC/C antagonist EMI1 inhibits UBE2S-mediated ubiquitin chain elongation on substrates by displacing the C-terminal extension from the APC2/4 grove (Frye et al., 2013; Wang and Kirschner, 2013). Whether this displacement affects Lys^{+5} ubiquitination of UBE2S has not been studied. However, interestingly, the autoubiquitination of Lys^{+5} in *UBC1*—a functional equivalent of UBE2S in yeast—was shown to be modulated by its nonconserved C-terminal extension *in vitro* (Hodgins et al., 1996). Finally, because Lys^{+5} ubiquitination does not trigger proteasomal degradation of UBE2S, it is tempting to speculate that specific DUBs can remove this modification, thus rendering this autoinhibition mechanism a reversible switch.

STAR★METHODS

Detailed methods are provided in the online version of this paper and include the following:

- KEY RESOURCES TABLE
- CONTACT FOR REAGENT AND RESOURCE SHARING
- EXPERIMENTAL MODEL AND SUBJECT DETAILS
- METHOD DETAILS
  - Gene Constructs
  - Protein Expression and Purification
  - Fluorophore-Labeling
  - Ubiquitination Assays
  - Preparation of UBE2S-Ubiquitin Conjugates
  - Nuclear Magnetic Resonance Spectroscopy
  - X-ray Crystallography
  - Molecular Dynamics Simulations
  - Cell Culture and Synchronization
  - UBE2S Immunoprecipitation
  - Cycloheximide Pulse-Chase Assay
  - Antibodies
  - Mass Spectrometry
- QUANTIFICATION AND STATISTICAL ANALYSIS
- DATA AND SOFTWARE AVAILABILITY

SUPPLEMENTAL INFORMATION

Supplemental Information can be found online at https://doi.org/10.1016/j.str.2019.05.008.

SUPPORTING CITATIONS

The following references appear in the Supplemental Information: Henikoff and Henikoff, 1992; McWilliam et al., 2013; The PyMOL Molecular Graphics System, n.d.; Waterhouse et al., 2009; Yates et al., 2017.

REFERENCES

Adams, P.D., Afonine, P.V., Bunkóczi, G., Chen, V.B., Davis, I.W., Echols, N., Headd, J.J., Hung, L.-W., Kapral, G.J., Grosse-Kunstleve, R.W., et al. (2010). PHENIX: a comprehensive Python-based system for macromolecular structure solution. Acta Crystallogr. D Biol. Crystallogr. *66*, 213–221.

Alfieri, C., Zhang, S., and Barford, D. (2017). Visualizing the complex functions and mechanisms of the anaphase promoting complex/cyclosome (APC/C). Open Biol. *7*, 170204.

Ayesha, A.K., Hyodo, T., Asano, E., Sato, N., Mansour, M.A., Ito, S., Hamaguchi, M., and Senga, T. (2015). UBE2S is associated with malignant characteristics of breast cancer cells. Tumor Biol. *37*, 763–772.

Bakos, G., Yu, L., Gak, I.A., Roumeliotis, T.I., Liakopoulos, D., Choudhary, J.S., and Mansfeld, J. (2018). An E2-ubiquitin thioester-driven approach to identify substrates modified with ubiquitin and ubiquitin-like molecules. Nat. Commun. *9*, 4776.

Banka, P.A., Behera, A.P., Sarkar, S., and Datta, A.B. (2015). RING E3-catalyzed E2 Self-ubiquitination attenuates the activity of Ube2E ubiquitin-conjugating enzymes. J. Mol. Biol. *427*, 2290–2304.

Ben-Eliezer, I., Pomerantz, Y., Galiani, D., Nevo, N., and Dekel, N. (2015). Appropriate expression of Ube2C and Ube2S controls the progression of the first meiotic division. FASEB J. *29*, 4670–4681.

Bocik, W.E., Sircar, A., Gray, J.J., and Tolman, J.R. (2011). Mechanism of polyubiquitin chain recognition by the human ubiquitin conjugating enzyme Ube2g2. J. Biol. Chem. *286*, 3981–3991.

Branigan, E., Plechanovová, A., Jaffray, E.G., Naismith, J.H., and Hay, R.T. (2015). Structural basis for the RING-catalyzed synthesis of K63-linked ubiquitin chains. Nat. Struct. Mol. Biol. *22*, 597–602.

Bremm, A., Freund, S.M.V., and Komander, D. (2010). Lys11-linked ubiquitin chains adopt compact conformations and are preferentially hydrolyzed by the deubiquitinase Cezanne. Nat. Struct. Mol. Biol. *17*, 939–947.

Brown, N.G., VanderLinden, R., Watson, E.R., Weissmann, F., Ordureau, A., Wu, K.-P., Zhang, W., Yu, S., Mercredi, P.Y., Harrison, J.S., et al. (2016). Dual RING E3 architectures regulate multiubiquitination and ubiquitin chain elongation by APC/C. Cell 165, 1440–1453.

Brown, N.G., Watson, E.R., Weissmann, F., Jarvis, M.A., VanderLinden, R., Grace, C.R.R., Frye, J.J., Qiao, R., Dube, P., Petzold, G., et al. (2014). Mechanism of polyubiquitination by human anaphase-promoting complex: RING repurposing for ubiquitin chain assembly. Mol. Cell 56, 246–260.

Brzovic, P.S., Lissounov, A., Christensen, D.E., Hoyt, D.W., and Klevit, R.E. (2006). A UbcH5/ubiquitin noncovalent complex is required for processive BRCA1-directed ubiquitination. Mol. Cell 21, 873–880.

Buetow, L., and Huang, D.T. (2016). Structural insights into the catalysis and regulation of E3 ubiquitin ligases. Nat. Rev. Mol. Cell Biol. 17, 626–642.

Buetow, L., Gabrielsen, M., Anthony, N.G., Dou, H., Patel, A., Aitkenhead, H., Sibbet, G.J., Smith, B.O., and Huang, D.T. (2015). Activation of a primed RING E3-E2-ubiquitin complex by non-covalent ubiquitin. Mol. Cell 58, 297–310.

Case, D.A., Ben-Shalom, I.Y., Brozell, S.R., Cerutti, D.S., Cheatham, T.E., Cruzeiro, I.V.W.D., Darden, T.A., Duke, R.E., Ghoreishi, D., Gilson, M.K., et al. (2018). AMBER 2018.

Chemical Computing Group (2018). Molecular Operating Environment (MOE) 2018.01 (ULC).

Chen, M.-F., Lee, K.-D., Lu, M.-S., Chen, C.-C., Hsieh, M.-J., Liu, Y.-H., Lin, P.-Y., and Chen, W.-C. (2009). The predictive role of E2-EPF ubiquitin carrier protein in esophageal squamous cell carcinoma. J. Mol. Med. 87, 307–320.

Chen, Z., and Ruffner, D.E. (1998). Amplification of closed circular DNA in vitro. Nucleic Acids Res. 26, 1126–1127.

Coccetti, P., Tripodi, F., Tedeschi, G., Nonnis, S., Marin, O., Fantinato, S., Cirulli, C., Vanoni, M., and Alberghina, L. (2008). The CK2 phosphorylation of catalytic domain of Cdc34 modulates its activity at the G1 to S transition in Saccharomyces cerevisiae. Cell Cycle 7, 1391–1401.

Darden, T., York, D., and Pedersen, L. (1998). Particle mesh Ewald: an N·log(N) method for Ewald sums in large systems. J. Chem. Phys. 98, 10089–10092.

Dou, H., Buetow, L., Sibbet, G.J., Cameron, K., and Huang, D.T. (2012). BIRC7-E2 ubiquitin conjugate structure reveals the mechanism of ubiquitin transfer by a RING dimer. Nat. Struct. Mol. Biol. 19, 876–883.

Duda, D.M., Scott, D.C., Calabrese, M.F., Zimmerman, E.S., Zheng, N., and Schulman, B.A. (2011). Structural regulation of cullin-RING ubiquitin ligase complexes. Curr. Opin. Struct. Biol. 21, 257–264.

Eddins, M.J., Carlile, C.M., Gomez, K.M., Pickart, C.M., and Wolberger, C. (2006). Mms2-Ubc13 covalently bound to ubiquitin reveals the structural basis of linkage-specific polyubiquitin chain formation. Nat. Struct. Mol. Biol. 13, 915–920.

Emsley, P., and Cowtan, K. (2004). Coot: model-building tools for molecular graphics. Acta Crystallogr. D Biol. Crystallogr. 60, 2126–2132.

Favier, A., and Brutscher, B. (2011). Recovering lost magnetization: polarization enhancement in biomolecular NMR. J. Biomol. NMR 49, 9–15.

Heinig, M., and Frishman, D. (2004). STRIDE: a web server for secondary structure assignment from known atomic coordinates of proteins. Nucleic Acids Res. 32, W500–W502.

Frye, J.J., Brown, N.G., Petzold, G., Watson, E.R., Grace, C.R.R., Nourse, A., Jarvis, M.A., Kriwacki, R.W., Peters, J.-M., Stark, H., et al. (2013). Electron microscopy structure of human APC/C-CDH1-EMI1 reveals multimodal mechanism of E3 ligase shutdown. Nat. Struct. Mol. Biol. 20, 827–835.

Garnett, M.J., Mansfeld, J., Godwin, C., Matsusaka, T., Wu, J., Russell, P., Pines, J., and Venkitaraman, A.R. (2009). UBE2S elongates ubiquitin chains on APC/C substrates to promote mitotic exit. Nat. Cell Biol. 11, 1363–1369.

Girard, J.R., Tenthorey, J.L., and Morgan, D.O. (2015). An E2 accessory domain increases affinity for the anaphase-promoting complex and ensures E2 competition. J. Biol. Chem. 290, 24614–24625.

Hamilton, K.S., Ellison, M.J., Barber, K.R., Williams, R.S., Huzil, J.T., McKenna, S., Ptak, C., Glover, M., and Shaw, G.S. (2001). Structure of a conjugating enzyme-ubiquitin thiolester intermediate reveals a novel role for the ubiquitin tail. Structure 9, 897–904.

Henikoff, S., and Henikoff, J.G. (1992). Amino-acid substitution matrices from protein blocks. Proc. Natl. Acad. Sci. U S A 89, 10915–10919.

Hibbert, R.G., Huang, A., Boelens, R., and Sixma, T.K. (2011). E3 ligase Rad18 promotes monoubiquitination rather than ubiquitin chain formation by E2 enzyme Rad6. Proc. Natl. Acad. Sci. U S A 108, 5590–5595.

Hodgins, R., Gwozd, C., Arnason, T., Cummings, M., and Ellison, M.J. (1996). The tail of a ubiquitin-conjugating enzyme redirects multi-ubiquitin chain synthesis from the lysine 48-linked configuration to a novel nonlysine-linked form. J. Biol. Chem. 271, 28766–28771.

Hornbeck, P.V., Zhang, B., Murray, B., Kornhauser, J.M., Latham, V., and Skrzypek, E. (2015). PhosphoSitePlus, 2014: mutations, PTMs and recalibrations. Nucleic Acids Res. 43, D512–D520.

Hu, L., Li, X., Liu, Q., Xu, J., Ge, H., Wang, H., Wang, Z., Shi, C., Xu, X., Huang, J., et al. (2017). UBE2S, a novel substrate of Akt1, associates with Ku70 and regulates DNA repair and glioblastoma multiforme resistance to chemotherapy. Oncogene 36, 1145–1156.

Hyberts, S.G., Milbradt, A.G., Wagner, A.B., Arthanari, H., and Wagner, G. (2012). Application of iterative soft thresholding for fast reconstruction of NMR data non-uniformly sampled with multidimensional Poisson Gap scheduling. J. Biomol. NMR 52, 315–327.

Izawa, D., and Pines, J. (2012). Mad2 and the APC/C compete for the same site on Cdc20 to ensure proper chromosome segregation. J. Cell Biol. 199, 27–37.

Johnson, B.A. (2004). Using NMRView to visualize and analyze the NMR spectra of macromolecules. Methods Mol. Biol. 278, 313–352.

Jorgensen, W.L., Chandrasekhar, J., Madura, J.D., Impey, R.W., and Klein, M.L. (1998). Comparison of simple potential functions for simulating liquid water. J. Chem. Phys. 79, 926–935.

Jung, C.-R., Hwang, K.-S., Yoo, J., Cho, W.-K., Kim, J.-M., Kim, W.H., and Im, D.-S. (2006). E2-EPF UCP targets pVHL for degradation and associates with tumor growth and metastasis. Nat. Med. 12, 809–816.

Kabsch, W. (2010). Integration, scaling, space-group assignment and post-refinement. Acta Crystallogr. D Biol. Crystallogr. 66, 133–144.

Kelly, A., Wickliffe, K.E., Song, L., Fedrigo, I., and Rape, M. (2014). Ubiquitin chain elongation requires E3-dependent tracking of the emerging conjugate. Mol. Cell 56, 232–245.

Knipscheer, P., Flotho, A., Klug, H., Olsen, J.V., Van Dijk, W.J., Fish, A., Johnson, E.S., Mann, M., Sixma, T.K., and Pichler, A. (2008). Ubc9 sumoylation regulates SUMO target discrimination. Mol. Cell 31, 371–382.

Labute, P. (2009). Protonate3D: assignment of ionization states and hydrogen coordinates to macromolecular structures. Proteins 75, 187–205.

Li, Z., Wang, Y., Li, Y., Yin, W., Mo, L., Qian, X., Zhang, Y., Wang, G., Bu, F., Zhang, Z., et al. (2018). Ube2s stabilizes beta-Catenin through K11-linked polyubiquitination to promote mesendoderm specification and colorectal cancer development. Cell Death Dis. 9, 456.

Liang, J., Nishi, H., Bian, M.-L., Higuma, C., Sasaki, M., Ito, H., and Isaka, K. (2012). The ubiquitin-conjugating enzyme E2-EPF is overexpressed in cervical cancer and associates with tumor growth. Oncol. Rep. 28, 1519–1525.

Lorenz, S. (2017). Structural mechanisms of HECT-type ubiquitin ligases. Biol. Chem. 399, 127–145.

Lorenz, S., Bhattacharyya, M., Feiler, C., Rape, M., and Kuriyan, J. (2016). Crystal structure of a Ube2S-ubiquitin conjugate. PLoS One 11, e0147550.

Machida, Y.J., Machida, Y., Chen, Y., Gurtan, A.M., Kupfer, G.M., D'Andrea, A.D., and Dutta, A. (2006). UBE2T is the E2 in the Fanconi anemia pathway and undergoes negative autoregulation. Mol. Cell 23, 589–596.

Maier, J.A., Martinez, C., Kasavajhala, K., Wickstrom, L., Hauser, K.E., and Simmerling, C. (2015). ff14SB: improving the accuracy of protein side chain and backbone parameters from ff99SB. J. Chem. Theory Comput. 11, 3696–3713.

McCoy, A.J., Grosse-Kunstleve, R.W., Adams, P.D., Winn, M.D., Storoni, L.C., and Read, R.J. (2007). Phaser crystallographic software. J. Appl. Crystallogr. 40, 658–674.

McWilliam, H., Li, W., Uludag, M., Squizzato, S., Park, Y.M., Buso, N., Cowley, A.P., and Lopez, R. (2013). Analysis tool web services from the EMBL-EBI. Nucleic Acids Res. *41*, W597–W600.

Metzger, M.B., Pruneda, J.N., Klevit, R.E., and Weissman, A.M. (2014). RING-type E3 ligases: master manipulators of E2 ubiquitin-conjugating enzymes and ubiquitination. Biochim. Biophys. Acta *1843*, 47–60.

Middleton, A.J., and Day, C.L. (2015). The molecular basis of lysine 48 ubiquitin chain synthesis by Ube2K. Sci. Rep. *5*, 16793.

Min, M., Mevissen, T.E.T., De Luca, M., Komander, D., and Lindon, C. (2015). Efficient APC/C substrate degradation in cells undergoing mitotic exit depends on K11 ubiquitin linkages. Mol. Biol. Cell *26*, 4325–4332.

Miura, T., Klaus, W., Gsell, B., Miyamoto, C., and Senn, H. (1999). Characterization of the binding interface between ubiquitin and class I human ubiquitin-conjugating enzyme 2b by multidimensional heteronuclear NMR spectroscopy in solution. J. Mol. Biol. *290*, 213–228.

Olsen, S.K., and Lima, C.D. (2013). Structure of a ubiquitin E1-E2 complex: insights to E1-E2 thioester transfer. Mol. Cell *49*, 884–896.

Page, R.C., Pruneda, J.N., Amick, J., Klevit, R.E., and Misra, S. (2012). Structural insights into the conformation and oligomerization of E2~ubiquitin conjugates. Biochemistry *51*, 4175–4187.

Pan, Y.-H., Yang, M., Liu, L.-P., Wu, D.-C., Li, M.-Y., and Su, S.-G. (2018). UBE2S enhances the ubiquitination of p53 and exerts oncogenic activities in hepatocellular carcinoma. Biochem. Biophys. Res. Commun. *503*, 895–902.

Papaleo, E., Ranzani, V., Tripodi, F., Vitriolo, A., Cirulli, C., Fantucci, P., Alberghina, L., Vanoni, M., De Gioia, L., and Coccetti, P. (2011). An acidic loop and cognate phosphorylation sites define a molecular switch that modulates ubiquitin charging activity in Cdc34-like enzymes. PLoS Comput. Biol. *7*, e1002056.

Petroski, M.D., and Deshaies, R.J. (2005). Mechanism of lysine 48-linked ubiquitin-chain synthesis by the cullin-RING ubiquitin-ligase complex SCF-Cdc34. Cell *123*, 1107–1120.

Phillips, J.C., Braun, R., Wang, W., Gumbart, J., Tajkhorshid, E., Villa, E., Chipot, C., Skeel, R.D., Kalé, L., and Schulten, K. (2005). Scalable molecular dynamics with NAMD. J. Comput. Chem. *26*, 1781–1802.

Pichler, A., Knipscheer, P., Oberhofer, E., Van Dijk, W.J., Körner, R., Olsen, J.V., Jentsch, S., Melchior, F., and Sixma, T.K. (2005). SUMO modification of the ubiquitin-conjugating enzyme E2-25K. Nat. Struct. Mol. Biol. *12*, 264–269.

Plafker, K.S., Nguyen, L., Barneche, M., Mirza, S., Crawford, D., and Plafker, S.M. (2010). The ubiquitin-conjugating enzyme UbcM2 can regulate the stability and activity of the antioxidant transcription factor Nrf2. J. Biol. Chem. *285*, 23064–23074.

Plechanovová, A., Jaffray, E.G., Tatham, M.H., Naismith, J.H., and Hay, R.T. (2012). Structure of a RING E3 ligase and ubiquitin-loaded E2 primed for catalysis. Nature *489*, 115–120.

Pruneda, J.N., Littlefield, P.J., Soss, S.E., Nordquist, K.A., Chazin, W.J., Brzovic, P.S., and Klevit, R.E. (2012). Structure of an E3:E2~Ub complex reveals an allosteric mechanism shared among RING/U-box ligases. Mol. Cell *47*, 933–942.

Pruneda, J.N., Stoll, K.E., Bolton, L.J., Brzovic, P.S., and Klevit, R.E. (2011). Ubiquitin in motion: structural studies of the ubiquitin-conjugating enzyme-~ubiquitin conjugate. Biochemistry *50*, 1624–1633.

Ranaweera, R.S., and Yang, X. (2013). Auto-ubiquitination of Mdm2 enhances its substrate ubiquitin ligase activity. J. Biol. Chem. *288*, 18939–18946.

Rape, M., and Kirschner, M.W. (2004). Autonomous regulation of the anaphase-promoting complex couples mitosis to S-phase entry. Nature *432*, 588–595.

Ravid, T., and Hochstrasser, M. (2007). Autoregulation of an E2 enzyme by ubiquitin-chain assembly on its catalytic residue. Nat. Cell Biol. *9*, 422–427.

Roe, D.R., and Cheatham, T.E., 3rd (2013). PTRAJ and CPPTRAJ: software for processing and analysis of molecular dynamics trajectory data. J. Chem. Theory Comput. *9*, 3084–3095.

Roos, F.C., Evans, A.J., Brenner, W., Wondergem, B., Klomp, J., Heir, P., Roche, O., Thomas, C., Schimmel, H., Furge, K.A., et al. (2011).

Deregulation of E2-EPF ubiquitin carrier protein in papillary renal cell carcinoma. Am. J. Pathol. *178*, 853–860.

RStudio Team. (2015). RStudio: Integrated Development for R (RStudio, Inc.). http://www.rstudio.com/.

Saha, A., Lewis, S., Kleiger, G., Kuhlman, B., and Deshaies, R.J. (2011). Essential role for ubiquitin-ubiquitin-conjugating enzyme interaction in ubiquitin discharge from Cdc34 to substrate. Mol. Cell *42*, 75–83.

Sako, K., Suzuki, K., Isoda, M., Yoshikai, S., Senoo, C., Nakajo, N., Ohe, M., and Sagata, N. (2014). Emi2 mediates meiotic MII arrest by competitively inhibiting the binding of Ube2S to the APC/C. Nat. Commun. *5*, 3667.

Sarcevic, B., Mawson, A., Baker, R.T., and Sutherland, R.L. (2002). Regulation of the ubiquitin-conjugating enzyme hHR6A by CDK-mediated phosphorylation. EMBO J. *21*, 2009–2018.

Sarkari, F., Wheaton, K., La Delfa, A., Mohamed, M., Shaikh, F., Khatun, R., Arrowsmith, C.H., Frappier, L., Saridakis, V., and Sheng, Y. (2013). Ubiquitin-specific protease 7 is a regulator of ubiquitin-conjugating enzyme UbE2E1. J. Biol. Chem. *288*, 16975–16985.

Schindelin, J., Arganda-Carreras, I., Frise, E., Kaynig, V., Longair, M., Pietzsch, T., Preibisch, S., Rueden, C., Saalfeld, S., Schmid, B., et al. (2012). Fiji: an open-source platform for biological-image analysis. Nat. Methods *9*, 676–682.

Sheng, Y., Hong, J.H., Doherty, R., Srikumar, T., Shloush, J., Avvakumov, G.V., Walker, J.R., Xue, S., Neculai, D., Wan, J.W., et al. (2012). A human ubiquitin conjugating enzyme (E2)-HECT E3 ligase structure-function screen. Mol. Cell. Proteomics *11*, 329–341.

Simpson, R.J. (2010). Disruption of cultured cells by nitrogen cavitation. Cold Spring Harb. Protoc. *2010*, https://doi.org/10.1101/pdb.prot5513.

Soss, S.E., Klevit, R.E., and Chazin, W.J. (2013). Activation of UbcH5c~Ub is the result of a shift in interdomain motions of the conjugate bound to U-box E3 ligase E4B. Biochemistry *52*, 2991–2999.

Stewart, M.D., Ritterhoff, T., Klevit, R.E., and Brzovic, P.S. (2016). E2 enzymes: more than just middle men. Nat. Publ. Group *26*, 423–440.

Stieglitz, B., Rana, R.R., Koliopoulos, M.G., Morris-Davies, A.C., Schaeffer, V., Christodoulou, E., Howell, S., Brown, N.R., Dikic, I., and Rittinger, K. (2013). Structural basis for ligase-specific conjugation of linear ubiquitin chains by HOIP. Nature *503*, 422–426.

Tedesco, D., Zhang, J., Trinh, L., Lalehzadeh, G., Meisner, R., Yamaguchi, K.D., Ruderman, D.L., Dinter, H., and Zajchowski, D.A. (2007). The ubiquitin-conjugating enzyme E2-EPF is overexpressed in primary breast cancer and modulates sensitivity to topoisomerase II inhibition. Neoplasia *9*, 601–613.

The PyMOL Molecular Graphics System, The PyMOL Molecular Graphics System, Version 2.0 Schrödinger, LLC.

Thompson, A., Schäfer, J., Kuhn, K., Kienle, S., Schwarz, J., Schmidt, G., Neumann, T., Johnstone, R., Mohammed, A.K.A., and Hamon, C. (2003). Tandem mass tags: a novel quantification strategy for comparative analysis of complex protein mixtures by MS/MS. Anal. Chem. *75*, 1895–1904.

Tsui, V., and Case, D.A. (2000). Theory and applications of the generalized born solvation model in macromolecular simulations. Biopolymers *56*, 275–291.

Tyanova, S., Temu, T., Carlson, A., Sinitcyn, P., Mann, M., and Cox, J. (2015). Visualization of LC-MS/MS proteomics data in MaxQuant. Proteomics *15*, 1453–1456.

UniProt Consortium, T (2018). UniProt: the universal protein knowledgebase. Nucleic Acids Res. *46*, 2699.

Valimberti, I., Tiberti, M., Lambrughi, M., Sarcevic, B., and Papaleo, E. (2015). E2 superfamily of ubiquitin-conjugating enzymes: constitutively active or activated through phosphorylation in the catalytic cleft. Sci. Rep. *5*, 14849.

van den Ent, F., and Löwe, J. (2006). RF cloning: a restriction-free method for inserting target genes into plasmids. J. Biochem. Biophys. Methods *67*, 67–74.

Vijay-Kumar, S., Bugg, C.E., and Cook, W.J. (1987). Structure of ubiquitin refined at 1.8 A resolution. J. Mol. Biol. *194*, 531–544.

Walden, H., and Rittinger, K. (2018). RBR ligase-mediated ubiquitin transfer: a tale with many twists and turns. Nat. Struct. Mol. Biol. *25*, 440–445.

Wang, W., and Kirschner, M.W. (2013). Emi1 preferentially inhibits ubiquitin chain elongation by the anaphase-promoting complex. Nat. Cell Biol. *15*, 797–806.

Waterhouse, A.M., Procter, J.B., Martin, D.M.A., Clamp, M., and Barton, G.J. (2009). Jalview version 2 - a multiple sequence alignment editor and analysis workbench. Bioinformatics *25*, 1189–1191.

Watson, E.R., Brown, N.G., Peters, J.-M., Stark, H., and Schulman, B.A. (2019). Posing the APC/C E3 ubiquitin ligase to orchestrate cell division. Trends Cell Biol. *29*, 117–134.

Wickliffe, K.E., Lorenz, S., Wemmer, D.E., Kuriyan, J., and Rape, M. (2011). The mechanism of linkage-specific ubiquitin chain elongation by a single-sub-unit E2. Cell *144*, 769–781.

Williamson, A., Banerjee, S., Zhu, X., Philipp, I., Iavarone, A.T., and Rape, M. (2011). Regulation of ubiquitin chain initiation to control the timing of substrate degradation. Mol. Cell *42*, 744–757.

Williamson, A., Wickliffe, K.E., Mellone, B.G., Song, L., Karpen, G.H., and Rape, M. (2009). Identification of a physiological E2 module for the human anaphase-promoting complex. Proc. Natl. Acad. Sci.U S A *106*, 18213–18218.

Winn, M.D., Ballard, C.C., Cowtan, K.D., Dodson, E.J., Emsley, P., Evans, P.R., Keegan, R.M., Krissinel, E.B., Leslie, A.G.W., McCoy, A., et al. (2011).

Overview of the CCP4 suite and current developments. Acta Crystallogr. D Biol. Crystallogr. *67*, 235–242.

Wood, A., Schneider, J., Dover, J., Johnston, M., and Shilatifard, A. (2005). The Bur1/Bur2 complex is required for histone H2B monoubiquitination by Rad6/Bre1 and histone methylation by COMPASS. Mol. Cell *20*, 589–599.

Wu, T., Merbl, Y., Huo, Y., Gallop, J.L., Tzur, A., and Kirschner, M.W. (2010). UBE2S drives elongation of K11-linked ubiquitin chains by the anaphase-promoting complex. Proc. Natl. Acad. Sci.U S A *107*, 1355–1360.

Yates, B., Braschi, B., Gray, K.A., Seal, R.L., Tweedie, S., and Bruford, E.A. (2017). Genenames.org: the HGNC and VGNC resources in 2017. Nucleic Acids Res. *45*, D619–D625.

Zerjatke, T., Gak, I.A., Kirova, D., Fuhrmann, M., Daniel, K., Gonciarz, M., Müller, D., Glauche, I., and Mansfeld, J. (2017). Quantitative cell cycle analysis based on an endogenous all-in-one reporter for cell tracking and classification. Cell Res. *19*, 1953–1966.

Zhang, Z., Yang, J., Kong, E.H., Chao, W.C.H., Morris, E.P., da Fonseca, P.C.A., and Barford, D. (2013). Recombinant expression, reconstitution and structure of human anaphase-promoting complex (APC/C). Biochem. J. *449*, 365–371.

STAR★METHODS

KEY RESOURCES TABLE

REAGENT or RESOURCE	SOURCE	IDENTIFIER
Antibodies		
Rabbit polyclonal anti-UBE2S antibody	this paper	N/A
Goat polyclonal anti-GFP antibody	MPI CBG Dresden, Germany	N/A
Mouse monoclonal anti-CSE1 antibody	Abcam	Cat# ab54674; RRID: AB_940806
Mouse monoclonal anti-α-tubulin antibody	Sigma-Aldrich	Cat# T5168; RRID: AB_477579
Rabbit monoclonal anti-HA tag antibody (clone C29F4)	Cell Signaling Technology	Cat# 3724; RRID: AB_1549585
Mouse monoclonal anti-ubiquitin (P4D1) antibody	Santa-Cruz Biotechnology	Cat# sc-8017; RRID: AB_628423
Horse anti-mouse IgG, HRP-linked antibody	Cell Signaling Technology	Cat# 7076; RRID: AB_330924
Goat anti-rabbit IgG, HRP-linked antibody	Cell Signaling Technology	Cat# 7074; RRID: AB_2099233
Donkey anti-mouse IgG, IRDye 800CW conjugated antibody	LI-COR Biosciences	Cat# 926-32212; RRID: AB_621847
Donkey anti-rabbit IgG, IRDye 800CW conjugated antibody	LI-COR Biosciences	Cat# 926-32213; RRID: AB_621848
Donkey anti-goat IgG, IRDye® 800CW conjugated antibody	LI-COR Biosciences	Cat# 926-32214; RRID: AB_621846
Donkey anti-mouse IRDye 680RD secondary antibody	LI-COR Biosciences	Cat# 926-68072; RRID: AB_10953628
Bacterial and Virus Strains		
E. coli Top10	Thermo Fisher Scientific	Cat# C404006
E. coli BL21 (DE3)	Thermo Fisher Scientific	Cat# C600003
E. coli Rosetta (DE3) pLysS	Merck	Cat# 70956-3
Chemicals, Peptides, and Recombinant Proteins		
BamHI	New England Biolabs	Cat# R0136
NotI	New England Biolabs	Cat# R0189
NheI	New England Biolabs	Cat# R0131
SmaI	New England Biolabs	Cat# R0141
UBE2S^{UBC} (1-156)	Wickliffe et al., 2011	N/A
UBE2S (1-222)	Wickliffe et al., 2011	N/A
ubiquitin	Wickliffe et al., 2011	N/A
ubiquitin K11R	Wickliffe et al., 2011	N/A
ubiquitin C0 (additional N-terminal Cys)	this paper	N/A
UBA1	Wickliffe et al., 2011	N/A
ubiquitin-cyclin B1^{NTD}	Brown et al., 2014	N/A
APC/C	Zhang et al., 2013	N/A
CDC20	Izawa and Pines, 2012	N/A
Strep-Tactin Superflow resin	IBA Life Sciences	Cat# 2-1208-002
Buffer E	IBA Life Sciences	Cat# 2-1000-025
IRDye 800CW maleimide	LI-COR Biosciences	Cat# 929-80020
thymidine	Sigma-Aldrich	Cat# T9250
taxol (Paclitaxel)	Sigma-Aldrich	Cat# T7191
MG132	VWR	Cat# 80053-196
iodoacetamide	Sigma-Aldrich	Cat# I1149
Complete protease inhibitor cocktail	Roche	Cat# 11836170001
PhosSTOP phosphatase inhibitors	Roche	Cat# 04906837001
Protein G Dynabeads	Thermo Fisher Scientific	Cat# 10004D
TEAB	Sigma-Aldrich	Cat# T7408
cycloheximide	VWR	Cat# 239764-1
RNAimax	Thermo Fisher Scientific	Cat# 13778150
TCEP	Sigma-Aldrich	Cat# 646547

(Continued on next page)

Continued

REAGENT or RESOURCE	SOURCE	IDENTIFIER
trypsin, MS grade	Thermo Fisher Scientific	Cat# 90057
TMT10plex™ isobaric label reagent set	Thermo Fisher	Cat# 90111
Stage Tips C18, 200 μL tips (discontinued now)	Thermo Fisher	Cat# SP301
DMEM/F12	Sigma-Aldrich	Cat# D6421
FBS	Thermo Fisher Scientific	Cat# 10270106
tetracycline	Sigma Aldrich	Cat# 87128-25G
penicillin streptomycin	Sigma-Aldrich	Cat# P0781
Glutamax	Thermo Fisher Scientific	Cat# 35050038
amphotericin B	Sigma-Aldrich	Cat# A2942
DMEM, high glucose, pyruvate	Thermo Fisher Scientific	Cat# 41966052
G418 (neomycin)	Sigma-Aldrich	Cat# G8168
Deposited Data		
Atomic coordinates and structure factors	Plechanovová et al., 2012	PDB: 4AP4
Atomic coordinates and structure factors	Wickliffe et al., 2011	PDB: 1ZDN
Atomic coordinates and structure factors	Lorenz et al., 2016	PDB: 5BNB
Atomic coordinates and structure factors	this paper	PDB: 6QHK
Atomic coordinates and structure factors	this paper	PDB: 6QH3
NMR backbone resonance assignments, UB2S^{UBC} C95S/C118M/K100C	this paper	BMRB: 27768
NMR backbone resonance assignments, disulfide-linked UB2S^{UBC} (C95S/C118M/K100C)-ubiquitin (G76C)-complex	this paper	BMRB: 27799
Mass spectrometric data	this paper	PRIDE: PXD012643
Experimental Models: Cell Lines		
hTERT RPE-1 mRuby-PCNA/histone3.1-iRFP	Zerjatke et al., 2017	N/A
HeLa K	Jonathon Pines, ICR, London/UK	RRID: CVCL_1922
SF9 insect cells	Expression Systems	N/A
Oligonucleotides		
wobbled, si-RNA-resistant, codon-optimized *UBE2S* gene ATGAATAGTAATGTCGAAAATTTGCCGCCCCATATAATAA GGTTAGTCTATAAAGAAGTCACCACCTTAACGGCCGATC CCCCGGACGGGATAAAAGTGTTCCCGAATGAAGAAGAT TTGACGGATTTGCAAGTGACGATAGAAGGGCCGGAAGG CACGCCCTACGCGGGCGGGTTATTTAGGATGAAGTTGT TATTAGGCAAAGATTTTCCGGCGAGTCCCCGAAAGGG TATTTTTTAACGAAAATATTTCACCCCAATGTCGGGGCG AACGGGGAAATATGTGTGAATGTCTTGAAACGCGATTG GACCGCGGAATTAGGGATAAGGCATGTCTTATTAACGA TAAAATGTTTATTAATACATCCGAATCCGGAGAGCGCCT TGAATGAAGAAGCCGGGAGGTTATTGCTCGAAAATTAT GAAGAATACGCCGCGAGAGCGAGGTTATTGACCGAAA TACATGGCGGGGCGGGGGGGCCCGTCGGGGCGCGCG GAGGCGGGGAGAGCGTTAGCGTCGGGGACGGAGGCG AGTAGTACGGATCCGGGCGCGCCCGGCGGGCCCGGC GGCGCGGAAGGGCCGATGGCGAAAAAACACGCGGGG GAAAGGGACAAAAAATTAGCCGCGAAAAAGAAAACCGA TAAAAAAAGAGCCTTAAGAAGATTATAG	Integrated DNA Technologies; this paper	N/A
UBE2S siRNA	Dharmacon	Cat# D-009707-02-0050
Oligonucleotides for sub-cloning and mutagenesis	Table S4	
Recombinant DNA		
UBE2S^{UBC} (1-156)	Wickliffe et al., 2011	N/A
UBE2S (1-222)	Wickliffe et al., 2011	N/A

Continued

REAGENT or RESOURCE	SOURCE	IDENTIFIER
ubiquitin	Wickliffe et al., 2011	N/A
ubiquitin K11R	Wickliffe et al., 2011	N/A
UBA1	Wickliffe et al., 2011	N/A
ubiquitin-cyclin B1^{NTD}	Brown et al., 2014	N/A
bacmid DNA encoding human APC/C	Zhang et al., 2013	N/A
bacmid DNA encoding human CDC20	Izawa and Pines, 2012	N/A
pIRES2-eGFP	Clontech	RRID: Addgene_60291
pcDNA5/FRT/TO-neo	Jonathon Pines, ICR, London/UK	RRID: Addgene_41000
pCDNA5 FRT/TO-MCS-IRES2-eGFP	this paper	N/A
Software and Algorithms		
Image Studio Software	LI-COR Biosciences	https://www.licor.com/bio/image-studio/
FiJi	Schindelin et al., 2012	https://imagej.net/Fiji/Downloads
RStudio	RStudio Team, 2015	N/A
Molecular Operating Environment 2018.01	Chemical Computing Group, ULC	https://www.chemcomp.com/
AMBERTools18	Case et al., 2018	http://ambermd.org/AmberTools.php
NAMD2.12	Phillips et al., 2005	http://www.ks.uiuc.edu/Research/namd/
PyMOL1.8.6	Schrödinger, LLC	https://www.schrodinger.com/suites/pymol/
Proteome Discoverer 2.2	Thermo Fisher Scientific	N/A
MaxQuant	Tyanova et al., 2015	https://www.maxquant.org/

CONTACT FOR REAGENT AND RESOURCE SHARING

Further information and requests for resources and reagents should be directed to and will be fulfilled by the Lead Contacts, Jörg Mansfeld (joerg.mansfeld@tu-dresden.de) and Sonja Lorenz (sonja.lorenz@virchow.uni-wuerzburg.de)

EXPERIMENTAL MODEL AND SUBJECT DETAILS

All purified proteins used in biochemical, biophysical, and structural experiments were recombinantly expressed in *E. coli* or in SF9 insect cells (see below). All genes are of human origin. hTERT RPE-1 mRuby-PCNA/histone3.1-iRFP cells, as described previously (Zerjatke et al., 2017), are a human female retina epithelial cell line, immortalized with human telomerase reverse transcriptase (hTERT). HeLa K cells, a kind gift from Jonathon Pines (ICR, London, UK), are a human cervical adenocarcinoma cell line from a 31 year-old female. Both cell lines were cultured according to standard mammalian tissue culture protocols and sterile techniques at 37°C in 5% CO_2 and tested in regular intervals for mycoplasma.

METHOD DETAILS

Gene Constructs
For *in vitro* studies UBE2S^{UBC} (1-156) and full-length UBE2S (1-222) were produced from a modified pSKB2 vector encoding the proteins with an N-terminal, ULP1-protease-cleavable His$_6$-tag (Wickliffe et al., 2011). For *cis/trans* assays, these constructs were modified to encode an additional N-terminal HA$_3$-tag. The constructs for the recombinant expression of untagged ubiquitin (in *E.coli*) and UBA1 (in insect cells) have previously been described (Wickliffe et al., 2011). To enable the maleimide-mediated labeling of ubiquitin by a fluorophore, the ubiquitin construct was modified to encode an additional N-terminal cysteine residue (Cys-1). The vector encoding the ubiquitin-cyclin B1^{NTD} fusion gene (N-terminal domain; residues 1-95, plus an engineered C-terminal cysteine residue) was kindly provided by Brenda Schulman, MPI of Biochemistry, Martinsried/Germany (Brown et al., 2014). The bacmid DNAs encoding the human APC/C was a kind gift from David Barford, ICR, London/UK (Zhang et al., 2013). The bacmid DNA encoding SBP-tagged CDC20 was a kind gift from Jonathon Pines, ICR, London/UK (Izawa and Pines, 2012). To enable siRNA-and-rescue experiments with untagged UBE2S and eGFP expressed from the same mRNA as a reporter, IRES-eGFP was excised from pIRES2-eGFP (Clontech) via BamHI/NotI and sub-cloned into the same sites of pcDNA5/FRT/TO-neo 1795) (a kind gift from Jonathon Pines (RRID: Addgene_41000) creating pCDNA5 FRT/TO-MCS-IRES2-eGFP. Subsequently, a wobbled si-RNA-resistant, codon-optimized Ube2S gene was synthesized (Integrated DNA Technologies, Coralville, IA/USA) (for the sequence, see Key Resources Table) and cloned into the NheI/SmaI sites of pCDNA5 FRT/TO-MCS-IRES2-eGFP.

All sub-cloning and mutagenesis was performed by ligation-during-amplification approaches (Chen and Ruffner, 1998; van den Ent and Löwe, 2006).

Protein Expression and Purification

UBE2S proteins and ubiquitin, in unlabeled and isotope-enriched forms, respectively, as well as UBA1 were prepared according to established protocols (Wickliffe et al., 2011). The preparation of the ubiquitin-cyclin B1^{NTD} fusion protein carrying an N-terminal GST and a C-terminal His$_6$-tag has also been described (Brown et al., 2014).

The APC/C was obtained from insect cells, as described previously (Zhang et al., 2013). Briefly, SF9 cells (Expression Systems, Davis, CA/USA) were co-infected with two recombinant baculoviruses (ratio 2:5; the first corresponding to the virus containing Strep-tagged APC4) encoding the APC/C at a multiplicity of infection (MOI) of ∼1 and a density of 1 million cells/ml and incubated at 27°C for 72 hours. Cell pellets were re-suspended in 50 mM Tris pH 8.3, 250 mM NaCl, 5 % glycerol, 1 mM EDTA, 2 mM DTT, 0.1 mM PMSF, 2 mM benzamidine, and 5 units/ml benzonase, protease inhibitor cocktail (Roche, Penzberg/Germany), disrupted by nitrogen cavitation (Simpson, 2010) in a 4639 Cell Disruption Vessel (Parr Instrument Company, Frankfurt/Germany), and the extract cleared by centrifugation. Strep-tagged APC/C was captured on Strep-Tactin Superflow resin (IBA Life Sciences, Göttingen/Germany), washed with 50 mM Tris pH 8.0, 250 mM NaCl, 5 % glycerol, 1 mM EDTA, 2 mM DTT, and 2 mM benzamidine, and eluted with buffer E (IBA Life Sciences) supplied with additional NaCl (final concentration 250 mM), 2 mM DTT, and 2 mM benzamidine, and purified by size-exclusion chromatography (Superose 6 Increase 10/300 GL column; GE Healthcare, Uppsala/Sweden) in 20 mM HEPES pH 8.0, 200 mM NaCl, 2 mM DTT, and 5 % glycerol.

The preparation of SBP-tagged CDC20 from SF9 cells (Expression Systems) was performed analogously to the above protocol used for the APC/C. In this case, protein elution from the affinity resin was conducted in buffer E (IBA Life Sciences) supplied only with NaCl (final concentration 250 mM), and glycerol was added to a final concentration of 10 % before flash-freezing the protein for storage.

Fluorophore-Labeling

To label ubiquitin at the N-terminus (Cys-1) and ubiquitin-cyclin B1^{NTD} at the C-terminus (Brown et al., 2014) with a fluorophore, the purified proteins were first incubated with 10 mM DTT for 10 minutes and desalted in 50 mM HEPES pH 7.0 and 150 mM NaCl. IRDye 800CW maleimide (LI-COR, Lincoln, NB/USA) was added to the proteins at 3-fold molar excess, the reactions incubated at room temperature for 2 hours, and then quenched with 10 mM DTT. To quantitatively remove unreacted fluorophores, the samples were desalted twice (HiPrep 26/10 desalting column; GE Healthcare), followed by an additional size-exclusion chromatography (Superdex 75 10/300 GL increase column; GE Healthcare) in 50 mM HEPES pH 7.0, 150 mM NaCl, and 2 mM DTT (ubiquitin-cyclin B^{NTD}) and 25 mM Tris pH 7.4, 100 mM NaCl, and 2 mM DTT (ubiquitin), respectively.

Ubiquitination Assays

Thioester formation between UBE2S and ubiquitin was monitored by mixing 0.25 μM E1 UBA1, 30 μM fluorophore-labeled ubiquitin (WT or K11R), 3 mM ATP, and 9 mM MgCl$_2$ in 25 mM Tris pH 7.0 and 100 mM NaCl. After 15 min on ice, 2 μM UBE2S was added. The reactions were incubated for 2 to 4 minutes at room temperature and quenched by addition of non-reducing SDS-PAGE loading dye; control reactions were quenched with reducing SDS loading dye. Samples were analyzed by SDS-PAGE and Coomassie staining.

To monitor UBE2S-driven isopeptide bond formation 0.25 μM UBA1, 2 μM UBE2S, 30 μM fluorophore-labeled ubiquitin, 3 mM ATP, and 7.5 mM MgCl$_2$ were incubated in 25 mM Tris pH 7.5 and 100 mM NaCl at 30°C for 30 min and 1 h, respectively. The reactions were quenched by addition of reducing SDS loading dye and monitored by SDS-PAGE combined with fluorescence imaging and Coomassie staining.

APC/C-dependent ubiquitination reactions were performed at 30°C in 30 mM HEPES pH 7.4, 175 mM NaCl, 8 mM MgCl$_2$, 0.05% Tween-20, 1 mM DTT, and 5% glycerol and contained 20 nM recombinant APC/C, 390 nM CDC20, 46 nM GST-UBA1, 280 nM UBE2S, 21 μM His$_6$-ubiquitin (WT or K11R), 2.6 mM ATP, 10 mM phosphocreatine, and 11 μM creatine kinase. For detection by fluorescence imaging, a labeled ubiquitin-cyclin B1 fusion substrate was used (see above). Reactions were quenched after the indicated times with reducing LDS loading dye (Thermo-Fisher, supplemented with 100 mM DTT) and subjected to SDS-PAGE.

To discriminate auto-ubiquitination of UBE2S in cis and *trans* 0.25 μM UBA1, 1 μM HA$_3$-UBE2S C95A (catalytically dead), 1 μM or 5 μM untagged UBE2S WT, 60 μM ubiquitin, 3 mM ATP, and 7.5 mM MgCl$_2$ were incubated in 25 mM Tris pH 7.0 and 100 mM NaCl at 30°C for 30 min and 1 h, respectively, quenched with reducing SDS loading dye, and analyzed by SDS-PAGE and anti-HA Western blotting.

Preparation of UBE2S-Ubiquitin Conjugates

For activity assays, a UBE2S-ubiquitin conjugate was isolated from an *in vitro* ubiquitination reaction. To this end 0.5 μM UBA1, 20 μM UBE2S^{UBC}, 120 μM ubiquitin K11R, 3 mM ATP, and 9 mM MgCl$_2$ were incubated in 25 mM Tris pH 7.0 and 100 mM NaCl at 30°C for 1 h. The reaction was subsequently diluted in 25 mM Tris pH 7.4 and 2 mM DTT to bring the salt concentration to 25 mM NaCl and the mono-ubiquitinated UBE2S species purified by anion exchange chromatography (Mono Q 4.6/100 PE; GE Healthcare) using a gradient from 25 to 500 mM NaCl in 25 mM Tris pH 7.4, and 2 mM DTT and a final size-exclusion chromatography (HiLoad 16/600 SD 75; GE Healthcare) in 25 mM Tris pH 7.4, 100 mM NaCl, and 2 mM DTT. The fraction of unmodified UBE2S^{UBC} from the reaction was also recovered and served as a control in our activity assays (Figure 3).

For NMR studies, disulfide-linked conjugates of ubiquitin (G76C) and UBE2S[UBC] (C95S/C118M/K100C) were prepared according to established protocols (Lorenz et al., 2016; Wickliffe et al., 2011). In short, the required purified protein variants were buffer-exchanged into 50 mM sodium phosphate pH 7.4 and ubiquitin activated by incubation with a 9-fold molar excess of 5,5'-dithio-bis-2-nitrobenzoic acid (DTNB) at room temperature for 40 min. Excess DTNB was then removed (HiPrep 26/10 desalting column; GE Healthcare) and the activated ubiquitin incubated with a sub-stoichiometric amount of the UBE2S[UBC] variant at room temperature for 30 minutes. After buffer exchange into 25 mM Tris pH 7.4 and 100 mM NaCl, the disulfide-linked complex was purified by anion exchange chromatography (MonoQ 4.6/100 PE; GE Healthcare) using a NaCl-gradient from 25 to 500 mM in 25 mM Tris pH 7.4 and subsequent size-exclusion chromatography (SD 75 16/600: GE Healthcare) in 75 mM sodium-phosphate pH 7.2 and 1 mM EDTA.

For chemical shift mapping, either of the components was supplied in a ^{15}N-enriched form; to generate backbone resonance assignments for the complex, both components were ^{15}N and ^{13}C-enriched.

Nuclear Magnetic Resonance Spectroscopy

Data were recorded at 25°C on a Bruker AVANCE IIIHD 700 MHz spectrometer equipped with a ^{1}H/^{15}N/^{13}C cryo-probe. All samples were in 75 mM sodium phosphate pH 7.2, 1 mM EDTA, 5 mM DTT, 2 mM TCEP (except for the disulfide-linked conjugate, which was kept in non-reducing conditions), and 10% D$_2$O. BEST-TROSY-based triple resonance data (Favier and Brutscher, 2011) were recorded for resonance assignment using non-linear sampling (NUS) with 25% of total data points. Data processing was performed with in-house software (K.S., Unpublished Data) based on the iterative soft thresholding method (Hyberts et al., 2012); NMRView (Johnson, 2004) was used for visualization and analysis. Backbone amide resonance assignments for ubiquitin G76C were derived from the Biological Magnetic Resonance Data Bank (BMRB) entry 17439 (Wickliffe et al., 2011). Backbone resonance signals for the UBE2S[UBC] C95S/C118M/K100C variant were assigned *de novo*, based on the triple resonance experiments using a 600 μM uniformly ^{15}N, ^{13}C protein sample. The signals of the disulfide-linked complex with ubiquitin G76C were assigned by comparison of the HSQC and HNCA spectra (400 μM ^{15}N, ^{13}C labeled protein sample) with the corresponding data from ubiquitin and the UBE2S[UBC] C95S/C118M/K100C variant. Due to missing signals, the following residues of the UBE2S[UBC] C95S/C118M/K100C variant could not be assigned: S3, N4, N11, and A90. Additionally, K18, E19, I31, H111, T115, R135 and L150 could not be unambiguously assigned in the context of the UBE2S[UBC]-Ub conjugate, due to signal overlap.

To study the UBE2S[UBC]-ubiquitin interactions in the context of the covalently linked conjugate we recorded ^{1}H-^{15}N-HSQC spectra of samples containing 200 μM conjugate, in which either the E2 component (UBE2S[UBC] C95S/C118M/K100C) or ubiquitin (G76C) was ^{15}N-enriched and compared these spectra to the corresponding ones for the *apo* protein components. Weighted combined chemical shift perturbations, $\Delta\delta(^1H^{15}N)$, were calculated according to the following equation:

$$\Delta\delta(^1H^{15}N) = \sqrt{\left(\delta(^1H) - \delta(^1H)_0\right)^2 + 0.04 \cdot \left(\delta(^{15}N) - \delta(^{15}N)_0\right)^2}$$

X-ray Crystallography

UBE2S[UBC] WT was crystallized at a concentration of 12 mg/ml at 20°C in sitting drops containing 0.2 M MgCl$_2$, 0.1 M Tris pH 8.5, 30% PEG 4000, 1 mM TCEP, and 0.67 mM phenylarsine oxide (PAO). Crystals were cryo-protected in the same solution including 10% glycerol. UBE2S[UBC] C118M was crystallized at a concentration of 18 mg/ml at 20°C in sitting drops containing 0.2 M MgCl$_2$, 0.1 M HEPES pH 7.5, and 25% PEG 3350. Crystals were cryo-protected in the same solution including 20% glycerol.

Diffraction data were collected at the European Synchrotron Radiation Facility (ESRF), Grenoble/France, beamline ID30A-3 (UBE2S[UBC] WT) and Deutsches Elektronen-Synchrotron (DESY), Hamburg/Germany, beamline P14 (UBE2S[UBC] C118M). The data were processed with XDS (Kabsch, 2010); molecular replacement was performed with Phaser (McCoy et al., 2007), as implemented in the Collaborative Computational Project No. 4 (ccp4) suite (Winn et al., 2011), using an available structure of UBE2S[UBC] (PDB: 1ZDN (Sheng et al., 2012)) as a search model. Refinement was performed with Phenix (Adams et al., 2010) and manual model building with Coot (Emsley and Cowtan, 2004).

Molecular Dynamics Simulations

The crystal structures of UBE2S[UBC] monomers (PDB: 1ZDN, 6QHK, and 6QH3) were prepared in MOE (Chemical Computing Group, 2018); water molecules and ions within 4.5 Å from the protein were kept, missing side chains added automatically, and protonation states at pH 7 determined by the Protonate3D (Labute, 2009) function. Topology and parameter files were built with the tleap module of AMBERTools18 (Case et al.). Energy minimization was carried out for 2,000 steps with an implicit water model (generalized Born implicit solvent model (Tsui and Case, 2000), using the sander.MPI module of AMBER18. After adding sodium ions for neutralization, the systems were solvated in a TIP3P water box (Jorgensen et al., 1998) with a minimum protein-to-box distance of 10 Å. The simulations were performed using NAMD 2.12 Nightly Build 2017-12-05 (Phillips et al., 2005) with AMBER ff14sb (Maier et al., 2015) forcefield parameters. Periodic boundary conditions were imposed and long-range electrostatics handled with the particle mesh Ewald methodology (PME) (Darden et al., 1998). 10,000 equilibration steps were carried out, followed by heating from 100 K to 300 K over 500 ps at a constant water box size. Harmonic constraints (0.5 kcal/(mol*Å^2)) were applied to non-solvent atoms for the first 100 ps and gradually lowered during the remaining heating process; afterwards the systems were allowed to move freely for another 500 ps. Two individual production simulations were performed for each equilibrated structure over 100 ns each at constant pressure (1.01325 bar, Nosé-Hoover Langevin piston pressure control) and constant temperature (300 K, Langevin

dynamics). 2 fs-time steps were used for integration, and coordinates for output trajectories saved every 500 steps (1 ps). Trajectory analysis was performed with CPPTRAJ: Trajectory Analysis, V18.01 (Roe and Cheatham, 2013).

Cell Culture and Synchronization
hTERT RPE-1 cells were maintained in DMEM/F12, supplemented with 10% fetal bovine serum (FBS), 1% penicillin-streptomycin, 1% Glutamax, 0.26% sodium bicarbonate, and 0.5 μg/mL amphotericin B. To generate stable cell lines expressing untagged siRNA-resistant UBE2S WT and UBE2S K^{+5}R, the endogenous hTERT RPE-1 mRuby-PCNA/histone3.1-iRFP (Zerjatke et al., 2017) cells were electroporated with a plasmid encoding either the WT UBE2S-IRES-eGFP or K^{+5}R UBE2S IRES-eGFP, followed by selection for stable integrants with 400 μg/ml neomycin (Sigma-Aldrich). Target protein expression was induced with 10 μg/ml tetracycline.

HeLa K cells were maintained in DMEM, supplemented with 10% FBS, 1% penicillin-streptomycin, 1% Glutamax, and 0.5 μg/mL amphotericin B. To obtain mitotic extracts, HeLa K cells were pre-synchronized at the border of G1 and S-phase with 2.5 mM thymidine (Sigma-Aldrich) for 24 h, followed by a 14 h-release in 117 nM taxol (Sigma-Aldrich) to arrest cells in prometaphase. Prometaphase cells were harvested by mitotic shake-off or released into DMEM for 30 or 120 min at 37°C before harvesting.

UBE2S Immunoprecipitation
Cell pellets were re-suspended in extraction buffer (0.5% NP40, 30 mM HEPES pH 7.4, 175 mM NaCl) supplemented with 10 μM MG132 (VWR, Radnor, PA/USA), 10 mM iodoacetamide (Sigma-Aldrich), complete protease inhibitor cocktail (Roche) and PhosSTOP phosphatase inhibitors (Roche) and incubated on ice for 15 min. Following centrifugation of cell debris, UBE2S was immunoprecipitated (IP) using a custom rabbit polyclonal anti-UBE2S antibody (generated against purified UBE2S^{UBC} by Moravian-Biotechnology Ltd., Brno, Czech Republic). To this end 260 μg of the antibody were coupled to 1 ml Protein G Dynabeads (Thermo-Fisher) according to the manufacturer's instructions. The UBE2S affinity resin was then equilibrated in the extraction buffer (see above), added to cell extracts at a ratio of 31.2 μg antibody to 10 mg extract and incubated at 4°C for 2 h. Subsequently, the resin was washed 3 times with the extraction buffer, 3 times with a high-salt buffer (1% NP40, 30 mM HEPES pH 7.4, 500 mM NaCl), 3 times with a low-salt buffer (30 mM HEPES pH 7.4, 50 mM NaCl) and 2 times with 100 mM TEAB buffer pH 8.5 (Sigma-Aldrich). For Western blot analysis, bound proteins were eluted from 1/40 part of the resin by addition of LDS loading dye (Thermo-Fisher), supplemented with 100 mM DTT, and boiled for 10 min.

Cycloheximide Pulse-Chase Assay
Tetracycline-inducible UBE2S-IRES-eGFPhTERT RPE-1 cells (UBE2S WT and K^{+5}R) were seeded in a 6-well plate (85500 cells/well) in media with or without tetracycline; in parallel, cells were transfected with UBE2S (ACAAGGAGGUGACGACACU) siRNA at a final concentration 25 nM, using RNAimax (Thermo Scientific) according to the manufacturer's instructions. After 48 h cells were treated with 355 μm cycloheximide (CHX; VWR, Radnor, PA/USA) for 1, 2, 4 or 6 h or with CHX and 10 μm MG132 for 6 h. Cells were harvested in LDS loading dye (Thermo-Fisher) supplemented with 100 mM DTT, boiled for 10 min, and analyzed by SDS-PAGE and Western blotting.

Antibodies
The following primary antibodies were used: UBE2S – custom rabbit polyclonal antibody; GFP – custom goat polyclonal antibody; CSE1 – AB54674 (Abcam, Cambridge/UK); α-tubulin – T5168 (Sigma-Aldrich); HA – C29F4 (Cell Signaling Technology, Danvers, MA/USA); ubiquitin – P4D1 (Santa-Cruz Biotechnology, Dallas, TX/USA). All secondary antibodies used are specified in the Key Resources Table.

Mass Spectrometry
To map ubiquitination sites in UBE2S by semi-quantitative mass spectrometry we set up *in vitro* ubiquitination reactions containing 0.25 μM UBA1, 5 μM UBE2S (UBE2S^{UBC} or full length UBE2S), 60 μM ubiquitin K11R, 3.5 mM ATP, and 7.5 mM MgCl$_2$ in 25 mM Tris pH 7.4 and 100 mM NaCl at 30°C for 1 hour, quenched them by addition of reducing loading dye and subjected them to SDS PAGE. Gel strips representing ubiquitinated UBE2S species were collectively excised and digested with trypsin. The extracted peptides were analyzed by nanoHPLC-coupled ESI-MS using a Q Exactive HF-mass spectrometer (Thermo Fisher Scientific, Waltham, MA, USA) under standard conditions with a TOP30 method. The separation time of the applied liquid chromatography gradient (10 to 45% of solvent B (80% (v/v) acetonitrile (ACN) and 0.08% formic acid) in solvent A (0.1% (v/v) formic acid)) was 43 minutes. Raw files were searched with the MaxQuant 1.6.3.3 software (Tyanova et al., 2015) against the human SwissProt database (UniProt Consortium T, 2018), supplemented with the recombinant protein sequences used in this study. Carbamidomethylation of cysteine residues was set as a fixed modification, and oxidation of methionines, acetylation of protein N-termini, and Gly-Gly-remnants at lysines were considered variable modifications.

For quantitative LC-MS/MS analysis of immunoprecipitated, resin-bound proteins (see section "UBE2S Immunoprecipitation") were re-suspended in 100 μl of digestion buffer (100 mM TEAB pH 8.5, 10 mM TCEP, 10 mM iodacetamide (Sigma-Aldrich, St. Louis, MI/USA)), incubated at room temperature for 1 hour, then supplied with 2.2 μg MS-grade trypsin (Thermo Fisher Scientific), and incubated at 37°C over night. Three replicates for each condition were performed. The resulting peptides were labeled with TMT10plex according to manufacturer's instructions (Thermo Fisher Scientific), mixed, dried in a SpeedVac (Thermo Fisher Scientific), resuspended in 5% ACN/0.1% formic acid (FA) and loaded to stage tips, followed by fractionation by step elution with 10%,

15%, 20%, and 50% ACN/0.1%FA. After drying in a SpeedVac, the peptides were resuspended in 0.5% FA for LC-MS/MS analysis using an Orbitrap Fusion Tribrid mass spectrometer coupled with U3000 RSLCnano UHPLC system. Both instruments and all columns described below are from Thermo Fisher Scientific. The peptides were first loaded on a PepMap C18 trap (100 μm i.d. x 20 mm, 100 Å, 5 μm) for 8 min at 10 μl/min with 0.1% FA/H_2O, then separated on a PepMap C18 column (75 μm i.d. x 500 mm, 100 Å, 2 μm) at 300 nl/min and a linear gradient of 4-36% ACN/0.1%FA for 90 min/cycle at 120 min for each fraction. Data were acquired using the MS2 method with Top Speed with 3 s of cycle time. The full MS scans (m/z 375-1500) were acquired at 120,000 resolution at m/z 200 and the AGC (Automatic Gain Control) set at 4e5 with 50 ms of maximum injection time. The most abundant multiply-charge ions (z = 3-5, above 2e5 counts) were then subjected to MS/MS fragmentation by HCD (Higher Collision Dissociation) (collision energy at 38%) with an isolation window at m/z 0.7 by quadrupole, detected in Orbitrap with 50,000 resolution, and AGC at 1e5 with 105 ms maximum injection time. The precursor ions had the m/z related to UBE2S-derived K^{+5}-containing tryptic peptide ions as the priority: 678.3769 (4+), 678.6229 (4+), 448.9376 (3+), 678.1309 (4+), 621.3322 (4+), 620.8401 (4+), 663.8755 (4+), 664.3675 (4+). The dynamic exclusion window was set to ±10 ppm with a duration of 15 s. Note, due to specific optimization of the mass spectrometry analysis prioritizing the precursor mass of Lys^{+5}-containing peptides, these might have been measured with better accuracy (smaller compression effect in the reporter ions) compared to unmodified peptides. This may have caused a small overestimation of the actual drop of Lys^{+5} peptides.

For quantitative LC-MS/MS analysis of individual gel bands, those were cut into small pieces and destained in 50% ACN/50mM TEAB including TCEP for reduction and iodoacetamide for alkylation. Gel pieces were then digested with trypsin overnight and the peptides extracted in 0.5% FA/50% ACN and dried in a SpeedVac. The extracted peptides were labeled by the TMT10plex reagent, as described above. The LC-MS/MS analysis was conducted as described above, except for the following parameters: the ACN/0.1% FA gradient was 4-32%; the intensity threshold of multiply charged ions for MS/MS was 5e4; no precursor ion was set as priority; and the dynamic exclusion window was set to 45 s.

Data Analysis: The LC-MS/MS data were processed with Proteome Discoverer 2.2 (Thermo Fisher Scientific) using the SequestHT to search against the reviewed Uniprot protein database of Homo sapiens plus the in-house contaminate database. The precursor mass tolerance was set at 10 ppm and the fragment ion mass tolerance at 0.1 Da. Spectra were searched for fully tryptic peptides with a maximum of one miss-cleavage. Carbamidomethyl (C) at cysteines and TMT6plex (peptide N-terminus) were set as static modifications; dynamic modifications included deamidation (N, Q), TMT6plex (K) and Gly-GlyTMT6plex (K) (343.206). Peptides were validated by Percolator with the q-value set at 0.05 for the Decoy database search. The search results were filtered by the Consensus step where the protein FDR was set at 0.01 (strict) and 0.05 (relaxed). The TMT10plex reporter ion quantifier used 20 ppm integration tolerance on the most confident centroid peak at the MS2 level. Only unique peptides were used for quantification.

QUANTIFICATION AND STATISTICAL ANALYSIS

Quantification of Coomassie stained gels, fluorescence-imaged gels, and Western blots detected with IRDye 800CW and IRDye 680RD secondary antibodies (LI-COR) were performed on a near-infrared fluorescence detection system (Odyssey, Li-COR) using the Image Studio Software (Li-COR). All quantifications are based on at least three independent repeats and show the mean and SDs, unless stated otherwise. Additional details are provided in the corresponding figure legends. No randomization or blinding was used in this study.

DATA AND SOFTWARE AVAILABILITY

The accession numbers for the atomic coordinates and structure factors reported in this paper are PDB: 6QHK and 6QH3. The accession numbers for the NMR backbone resonance assignments for UB2S^{UBC} C95S/C118M/K100C and the disulfide-linked UB2S^{UBC} (C95S/C118M/K100C)-ubiquitin (G76C)-complex are BMRB: 27768 and 27799. The accession number for the mass spectrometric data is PRIDE: PXD012643.